Supporting information for:

Spontaneous Magnetic Field Enhancement in Nano-frameworks Enables Efficient ORR

Zhijie Qi[a], Zhenjie Lu[a], Pengcheng Yao[,b], Wuxin Bai[a], Lianjin Wei[a], Duansheng Liu[a], Jun Jiang[a], Shujun Liu[a], Pawel J. Kulesza[c], Jingwen Sun[a], Xin Wang[a], Junwu Zhu*[,a] and Yongsheng Fu[*,a]*

[a]*Key Laboratory for Soft Chemistry and Functional Materials, School of Chemistry and Chemical Engineering, Nanjing University of Science and Technology, Nanjing 210094, China*

[b]*Department of Chemical and Biomolecular Engineering and Ralph O'Connor Sustainable Energy Institute, Johns Hopkins University, Baltimore, Maryland 21218, United States*

[c]Faculty of Chemistry, University of Warsaw, Pasteura 1, PL 02-093 Warsaw, Poland

*Corresponding author.

E-mail: pyao4@jh.edu; zhujw@njust.edu.cn; fuyongsheng@njust.edu.cn

Method

Chemicals

All chemicals are purchased and used commercially and require no further purification.

Synthetic procedure

Synthesis of ZIF-67. Following the previous report, 0.30 g of $Co(NO_3)_2{\cdot}6H_2O$ and 5 mg of CTAB were added to 10 mL of deionized water, and the mixture was sonicated for 5 minutes to form a clear solution A. Then, 4.54g of dimethylimidazole was added to 70 mL of deionized water and stirred to form solution B. Solution A was poured into solution B and stirred for 20 minutes and then to precipitate at room temperature for 24 hours. The resulting solution was centrifuged, and the obtained ZIF-67 cubes were subjected to multiple alcohol washes.

Preparation of ZIF-L NFs. Similar to the above steps for the synthesis of ZIF-67, but after standing for 24h, 70 mL of supernatant was removed from the solution and 10 μL of remaining mother liquor was transferred to the silicon plate (10 mm × 10 mm) at room temperature to form droplets. ZIF-L NFs were obtained after the droplets were naturally dried.

Preparation of H-ZIF-67. 10 mg of ZIF-67 was dispersed in 5 mL of deionized water. Then, 5 mL of 10 g/L TA solution was added to the ZIF-67 suspension and allowed to stand for 5 minutes. The product was then centrifuged three times with ethanol and dried in a vacuum oven at 60°C overnight to obtain H-ZIF-67.

Preparation of Co@NC-NFs, Co@NC-H and Co@NC. The obtained ZIF-L NFs are placed in a ceramic boat, heated to 500 ℃ at a ramp rate of 2 ℃ min^{-1}, and maintained for 2 h in a tube furnace under nitrogen atmosphere. After that, the furnace is cooled

down to room temperature naturally. The preparation method of Co@NC and Co@NC-H are similar to the above procedure, except that the precursors of pyrolysis are ZIF-67 and H-ZIF-67.

Preparation of $CoPt_3$@NC-NFs and $CoPt_3$@NC. 50 mg of $CoPt_3$@NC-NFs and 10 mL of 10 mg mL^{-1} K_2PtCl_4 water solution were added to 40 mL of deionized water under magnetic stirring. The resulting solution was stirred for 48 h. Then it was centrifuged and dried at 60 °C under vacuum overnight. The powder sample was placed in a tube furnace, heated to 700 °C with a heating rate of 2 °C·min^{-1} under a flowing of N_2, holding for 2 h, and then cooled to room temperature naturally to get $CoPt_3$@NC-NFs. The preparation method of $CoPt_3$@NC and $CoPt_3$@NC-H is similar to the above procedure, except that the precursors of pyrolysis are Co@NC and Co@NC-H.

Materials Characterizations

Field emission scanning electron microscopy (FESEM, Quanta 400 FEG) equipped with energy-dispersive X-ray spectroscopy (EDS) , transmission electron microscopy (TEM, JEOL JEM-2100) operated at 200 kV), and high-resolution TEM (HRTEM) (FEI Talos F200X G2) equipped with EDS (FEI SuperX G2) were used to study the microscopic morphology and crystal structure of these samples. The structure of these samples was recorded using an X-ray diffractometer Bruker D8 Advance diffractometer (Miniflex-600W, Rigaku Corporation, Tokyo, Japan) with Cu Kα (λ = 0.15406 nm) radiation over a scan angle (2θ) range of 5° to 80°. The Raman measurement was to record the Raman spectrum using a laser with a wavelength of 532 nm as a detector. The X-ray photoelectron spectroscopy (XPS) was carried out to analyze the element

composition and binding energy of these samples surface by using Thermo ESCALAB 250 spectrometer with Al Kα (1486.6 eV) as excitation source.

Electrochemical measurements

A typical three-electrode system with an Auto-Lab electrochemical workstation (PGSTAT302N, Switzerland) was carried out explore electrochemical properties of the catalysts towards ORR. The oxygenated 0.1 M KOH solution was used as electrolyte, and the prepared samples were used as the working electrode, while a Ag/AgCl electrode and a carbon rod electrode were used as the reference and counter electrodes, respectively. The catalyst ink was prepared by ultrasonically dispersing 1 mg of catalysts in the mixture of isopropanol (125 uL) and Nafion (3 μL, 5 wt. %) to form a homogeneous suspension. 15 μL of the catalyst ink was then loaded onto the polished GC surface and dried at room temperature.

The performance of oxygen reduction reaction (ORR) was evaluated using cyclic voltammetry (CV) and rotating disk electrode (RDE) techniques. CV tests were conducted in a 0.1 M KOH electrolyte saturated with N_2/O_2, with a scan rate of 10 mV/s. Linear sweep voltammetry (LSV) polarization curves of the O_2-saturated electrolyte were measured at a scan rate of 5 mV/s under a rotation speed of 1600 rpm. Additionally, LSV polarization curves at different speeds were obtained using RDE with a scan rate of 5 mV/s in the range of 400 to 1600 rpm.

All the potentials reported in the results and discussion were measured against Ag/AgCl electrode and normalized to reversible hydrogen electrode (RHE) according to the formula:

$$E(RHE) = E_0 + E_{Ag/AgCl} + 0.0592pH \quad (1)$$

where E_0 is the measured potential vs. Ag/AgCl, $E_{Ag/AgCl}$ is 0.098 V.

Calculation of electron transfer number (n) and H_2O_2% for ORR

On the basis of RDE data, the electron transfer number per oxygen molecule involved in oxygen reduction can be determined by Koutechy-Levich equation:

$$\frac{1}{j} = \frac{1}{j_L} + \frac{1}{j_K} = \frac{1}{B\omega^{1/2}} + \frac{1}{j_K} \quad (2)$$

where j_K is the kinetic current and ω is the electrode rotating rate. B is determined from the slope of the Koutechy-Levich (K-L) plots according to the Levich equation as given below:

$$B = 0.2nFC_0D_0^{2/3}\upsilon^{-1/6} \quad (3)$$

where n represents the transferred electron number per oxygen molecule. F is Faraday constant (F = 96485 C mol^{-1}). is the diffusion coefficient of O_2 in 0.1 M KOH (D_0 = 1.9 × 10^{-5} cm^2 s^{-1}). is the kinetic viscosity (υ = 0.01 cm^2 s^{-1}). C_0 is the bulk concentration of O_2 (C_0 = 1.2 × 10^{-6} mol cm^{-3}). The constant 0.2 is adopted when the rotation speed is expressed in rpm.

For the RRDE measurements, the disk electrode was scanned at a rate of 5 mV s^{-1}, and the ring potential was constant at 1.3 V vs. RHE. The % and transferred electron number per oxygen molecule (n) were determined by the followed equations:

$$n_{RRDE} = 4 \times \frac{i_d}{i_d + \frac{i_r}{N_c}} \quad (4)$$

$$\%H_2O_2 = 100 \times \frac{\frac{2i_r}{N_c}}{i_d + \frac{i_r}{N_c}} \quad (5)$$

Where i_d is disk current, i_r is ring current, and N_c is current collection efficiency of the Pt ring. was determined to be 0.37.

Zn-air battery measurement

In order to further evaluate the electrochemical performance of the prepared Co@CNTs@NG catalyst, a homemade Zn-air battery was assembled. The zinc-air battery uses catalyst coated carbon paper (about 1.25 $mg \cdot cm^{-2}$) as the air cathode, polished Zn plate as the anode, and 6 M KOH + 0.2 M $Zn(OAc)_2 \cdot 2H_2O$ solution as the electrolyte.

DFT calculation details

All spin-polarized DFT calculations were performed using the VASP with the projector augmented wave (PAW) method.[1,2] The exchange-correlation functional was treated within the generalized gradient approximation (GGA) in the form of Perdew-Burke-Ernzerhof (PBE).[3,4] The Kohn-Sham states were expanded in a plane wave basis set with an energy cutoff of 400 eV. The convergence criteria for energy was set to 10^{-5} eV, and for forces it was set to 0.02 eV/Å during the structural optimization. The calculation employs a 2 x 2 x 1 grid mesh for K-space sampling. To account for van der Waals interactions, the DFT-D3 method with Becke-Johnson damping was applied. Given the paramagnetic nature of O_2 and the ferromagnetic properties of $CoPt_3$, all calculations were conducted with spin polarization enabled. The Gibbs free energy changes (ΔG) for ORR intermediates were calculated following the standard computational hydrogen electrode (CHE) model, with corrections for zero-point energy and entropic contributions at 298.15 K.

For the construction of the surface model, A vacuum of 20 Å is used to eliminate the interaction between the periodic structures. According to the observation of the

strongest diffraction peak in the (111) plane of $CoPt_3$ in the XRD pattern, the (111) plane of $CoPt_3$ model is selected for modeling. For better comparison, Pt and CoPt also selected (111) crystal plane for modeling.

The Gibbs free energy profiles of reaction pathways were calculated based on the standard hydrogen electrode (SHE) model. The adsorption Gibbs free energies of reaction intermediates for each step of the oxygen reduction reaction (ORR) were obtained using the following approach/company.

$$\Delta G = \Delta E + \Delta ZPE - T\Delta S + eU \qquad (6)$$

Where ΔG is the binding energy of different adsorption species, ZPE is the zero point energy, T is the temperature, ΔS is the entropy change, and U is the applied potential.

Multi fields simulation details

The distribution of magnetic field intensity and extended distribution of oxygen on the prepared $CoPt_3$@NC-NFs and $CoPt_3$@NC electrode were simulated by COMSOL Multiphysics. The nano-cubic and nano-frameworks models were established at 500 *500 *500 nm. Magnetic field module and fluid flow particle tracking module were used for simulation. The detail for simulation is given below: (I) The applied currents is 0-10 nA, (II) 0.1 M KOH is the electrolyte. (III) The fluid flow particle is set with the properties of O_2.

SECM Measurements

The SECM experiment was conducted using a four-electrode system controlled by a double potentiostat (Guangdong Dynechem Electronics Technology Co., Ltd., China). Pt disk electrode sealed in a glass capillary (Φ = 10 μm) is used as the SECM tip

electrode, and the catalysts coated on the glass carbon (GC) disk is used as the working electrode. In order to prepare the catalysts working electrode, 2.5 mg of catalysts was dispersed in 1 mL of deionized water, ethanol, and Nafion (5 wt %) (49:49:2 by volume) and then ultrasonically treated for 30 min to form a uniform dispersion. Next, 2 μL of dispersion was dripped onto the surface of glass carbon (Φ = 3 mm) and dried naturally at room temperature. Pt wire and Hg/HgO were used as the counter electrode and reference electrode, respectively. In the experimental scheme, the feedback mode of SECM was used to execute the approach curves, keeping the potential of the SECM tip electrode at −0.3 V vs Hg/HgO and the catalysts working electrode at the open-circuit potential. The distance between the tip electrode and the catalysts working electrode is controlled at 10 μm. 0.1 M KCl was used as the supporting electrolyte in 5 mM $K_3[Fe(CN)_6]$ as a mixed solution. The CV curves were recorded in the potential window of −0.1 to 0.5 V vs Hg/HgO. The CV curves and the approach curves are tested in the mixed solution.

The two-dimensional scanning electrochemical microscope images of catalysts working electrode were obtained in the feedback mode. In a typical experiment, the current varied with a minute distance between the tip electrode and the surface of the catalysts working electrodes, which can be used to obtain the microscopic distribution of the electrode materials in a 3 × 3 mm^2. For the TG/SG mode, the tip–substrate distance was first maintained as in the above measurements, while the electrolyte was replaced with 0.1 M KOH, and the potential of the catalyst electrode was held at 0.6 V vs RHE,. The Pt tip electrode was held at 1.3 V vs RHE.Furthermore, both tests were

performed using a serpentine scan in the x-y plane at a probe height of 10 μm. The scan step size was 10 μm, and the dwell time for each pixel was 5 s.

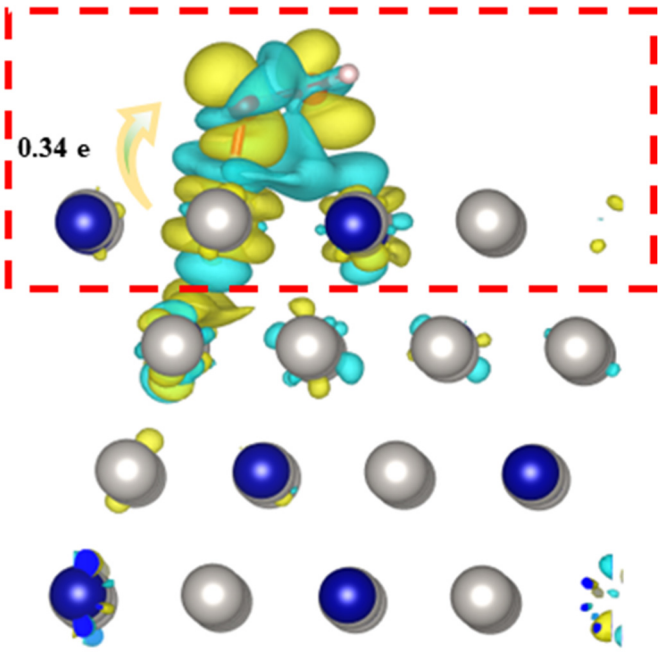

Figure S1 Differential charge diagram of *OOH on $CoPt_3$.

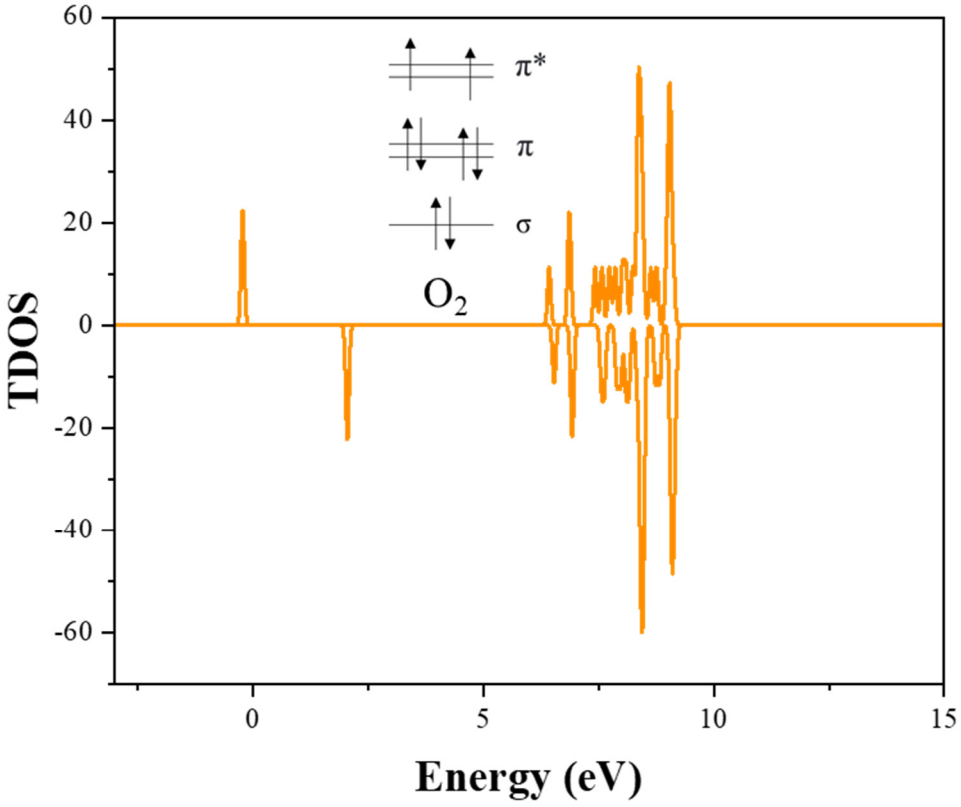

Figure S2 TDOS of O_2.

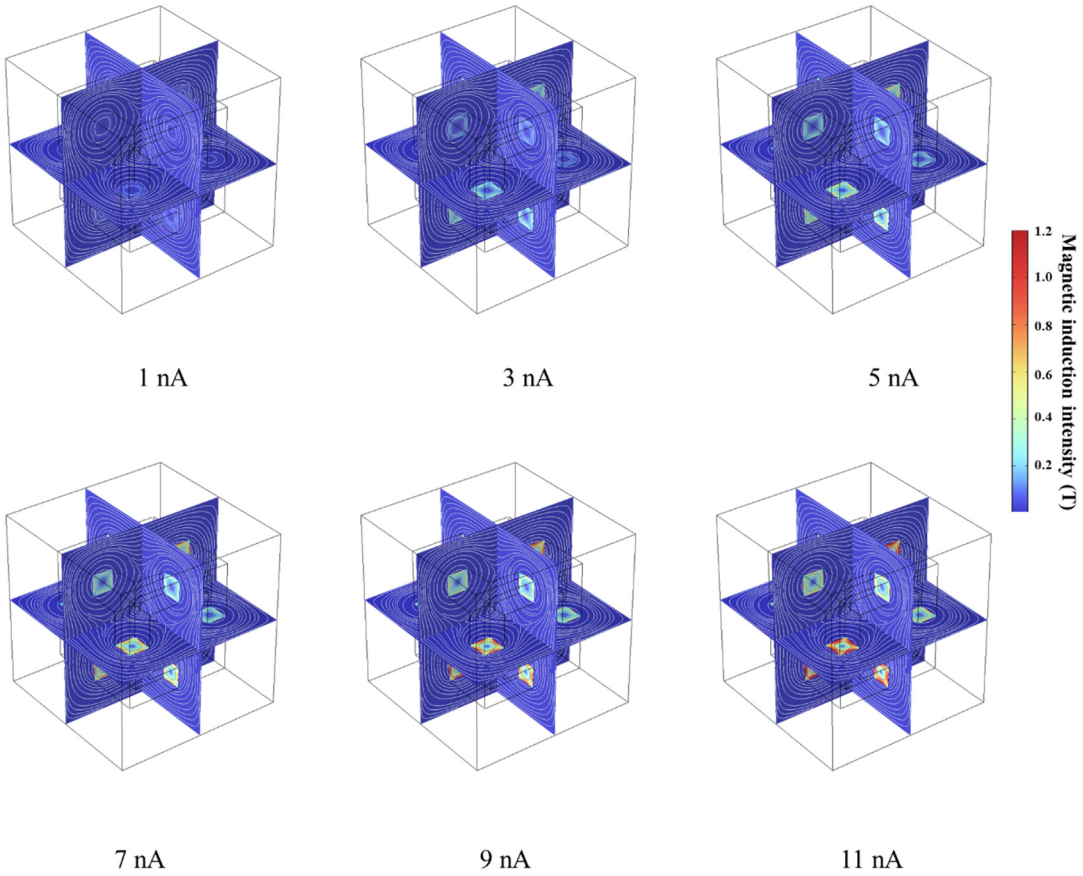

Figure S3 Surface magnetic field generated by frame model at different current.

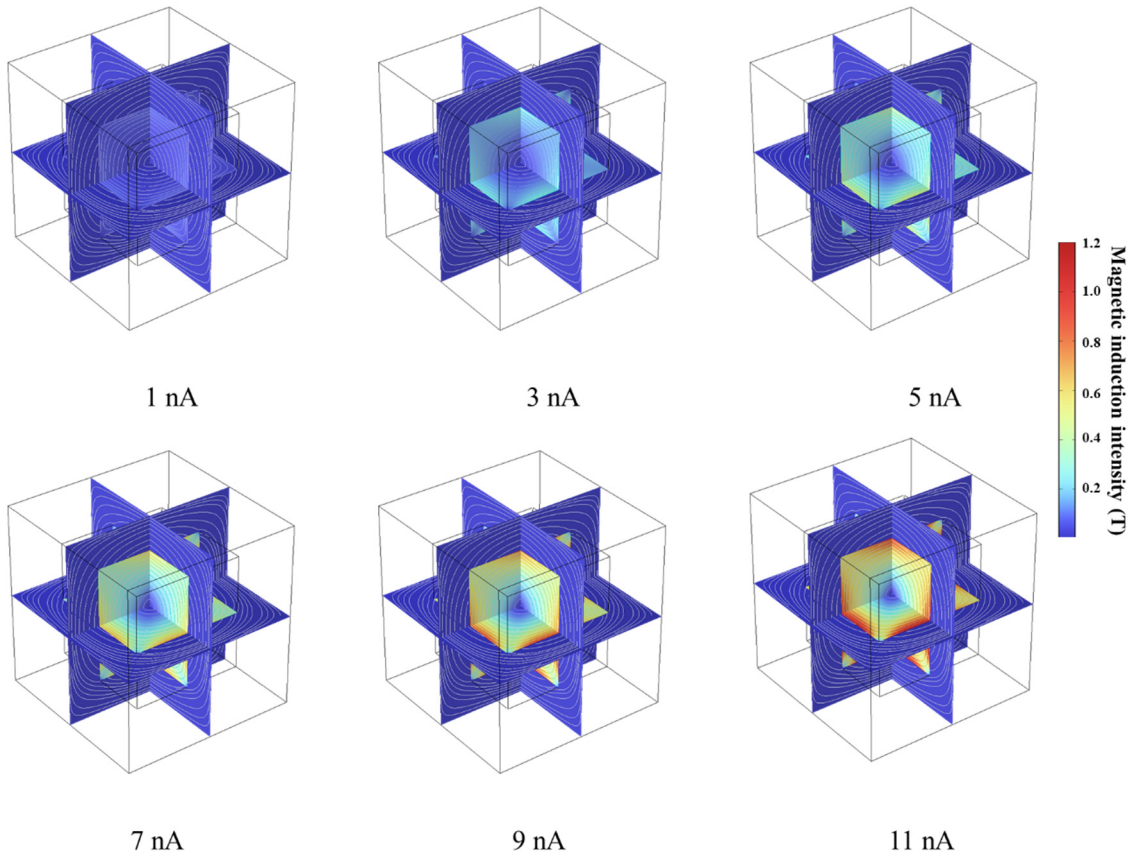

Figure S4 Surface magnetic field generated by cubic model at different current.

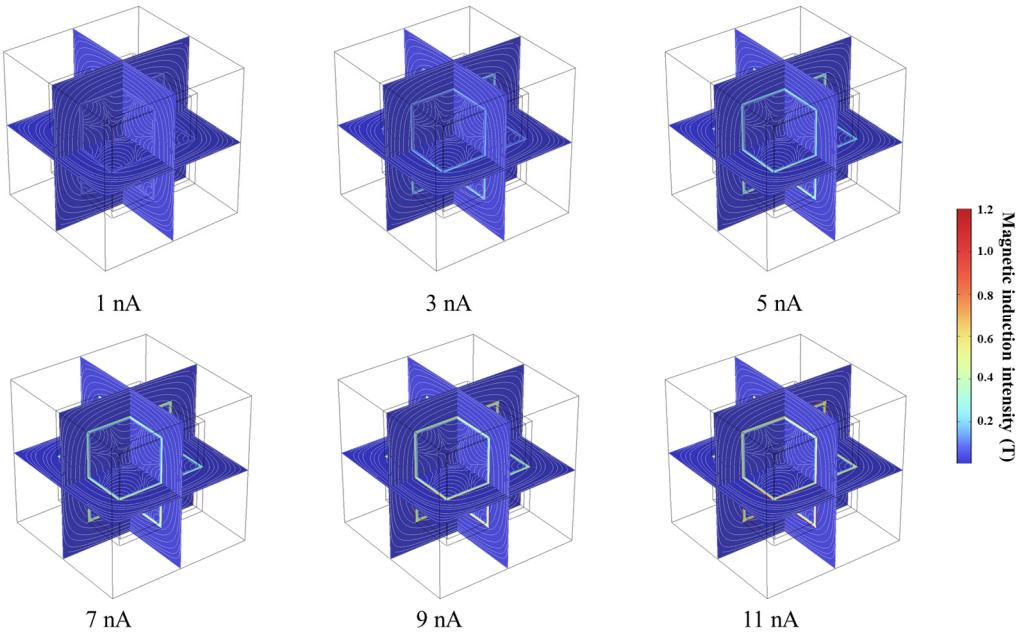

Figure S5 Surface magnetic field generated by hollow model at different current.

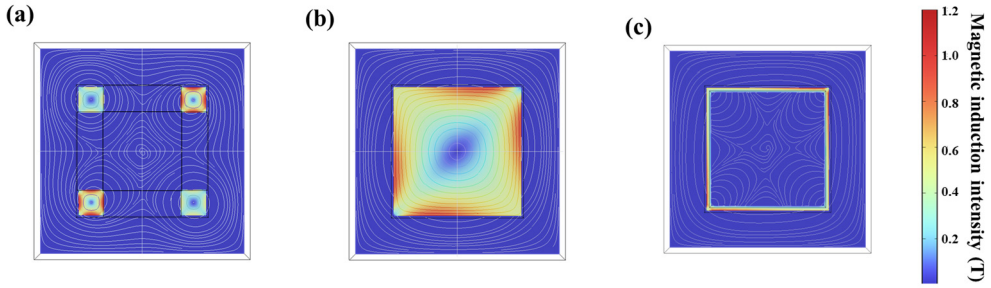

Figure S6 Magnetic field distribution of XY plane of framework (a), cube (b) and hollow (c) model.

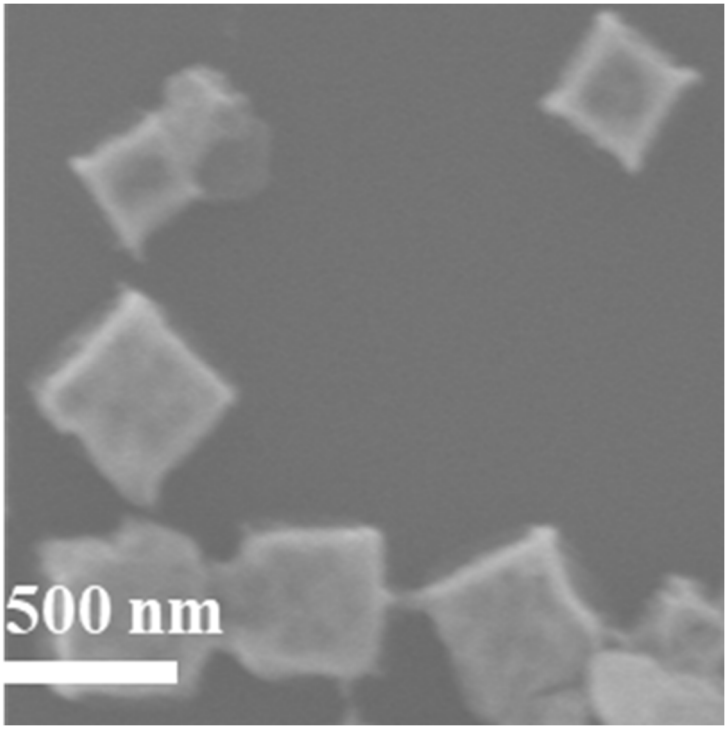

Figure S7 SEM image of $CoPt_3$@NC.

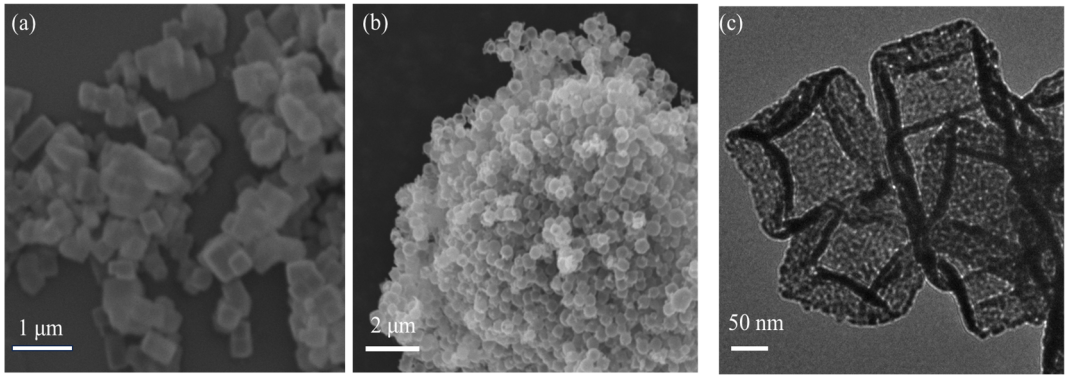

Figure S8 SEM image of H-ZIF-67 (a), $CoPt_3$@NC-H (b), TEM image of $CoPt_3$@NC-H.

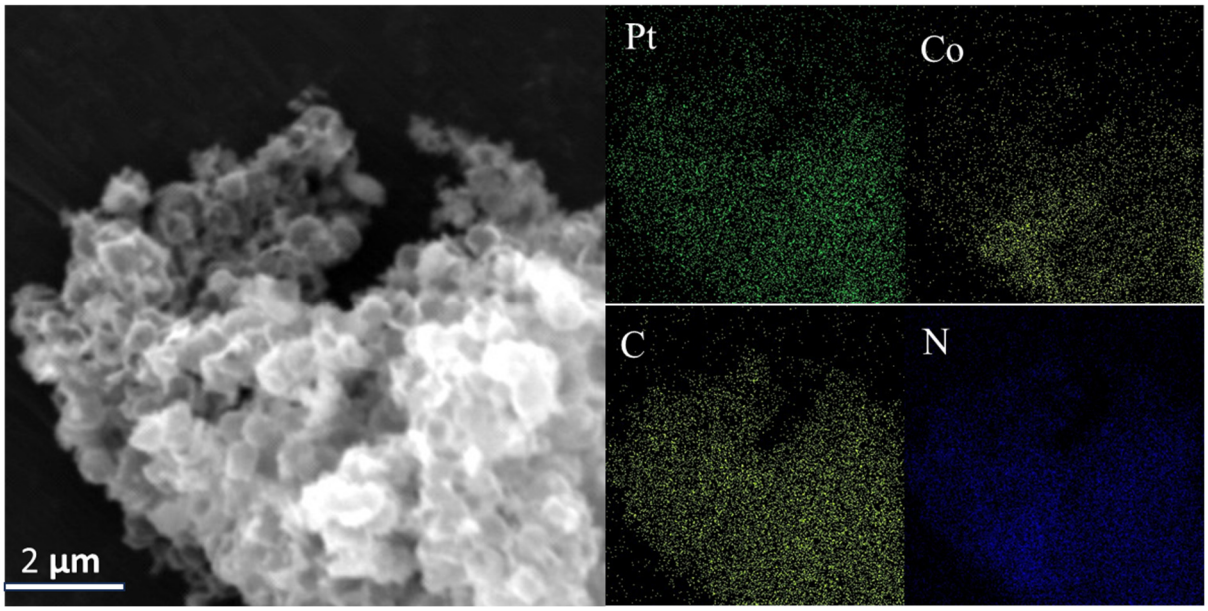

Figure S9 SEM image and mapping of $CoPt_3$@NC-H.

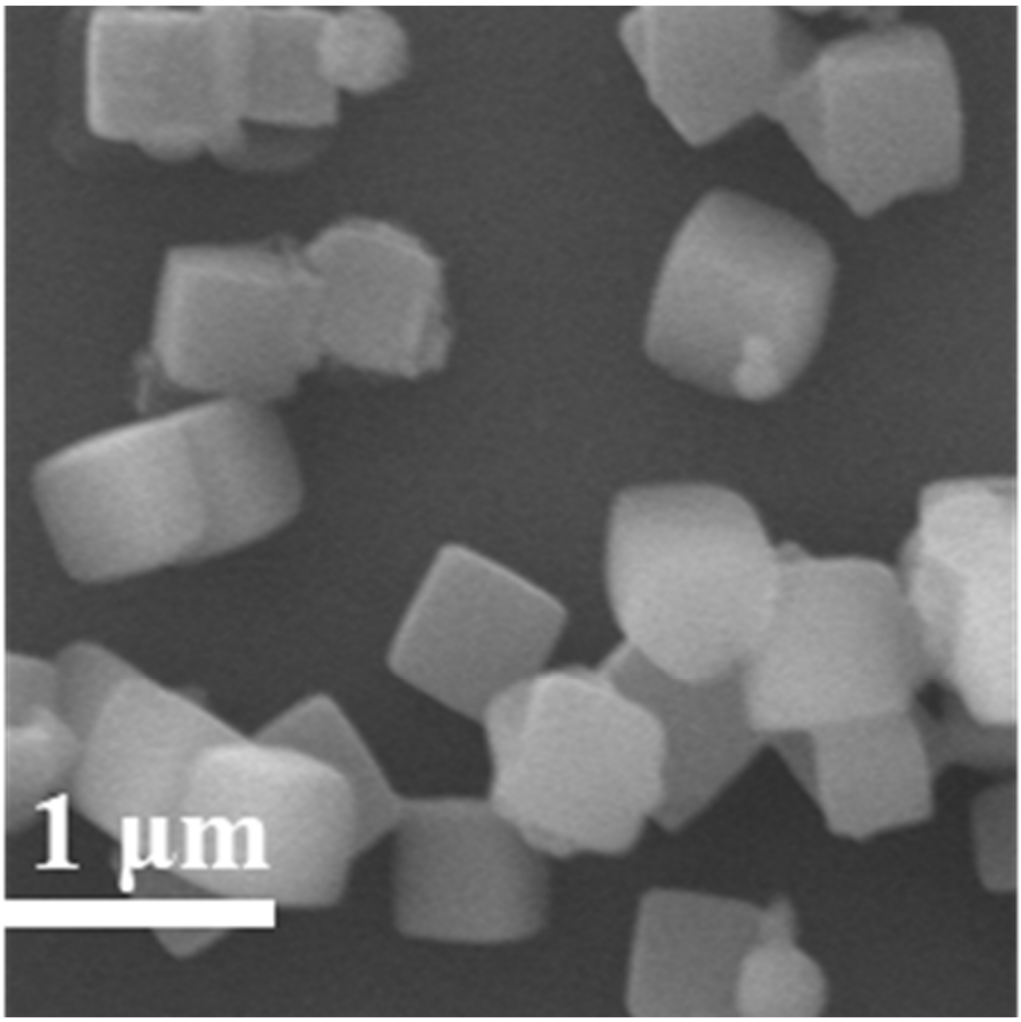

Figure S10 SEM image of ZIF-67

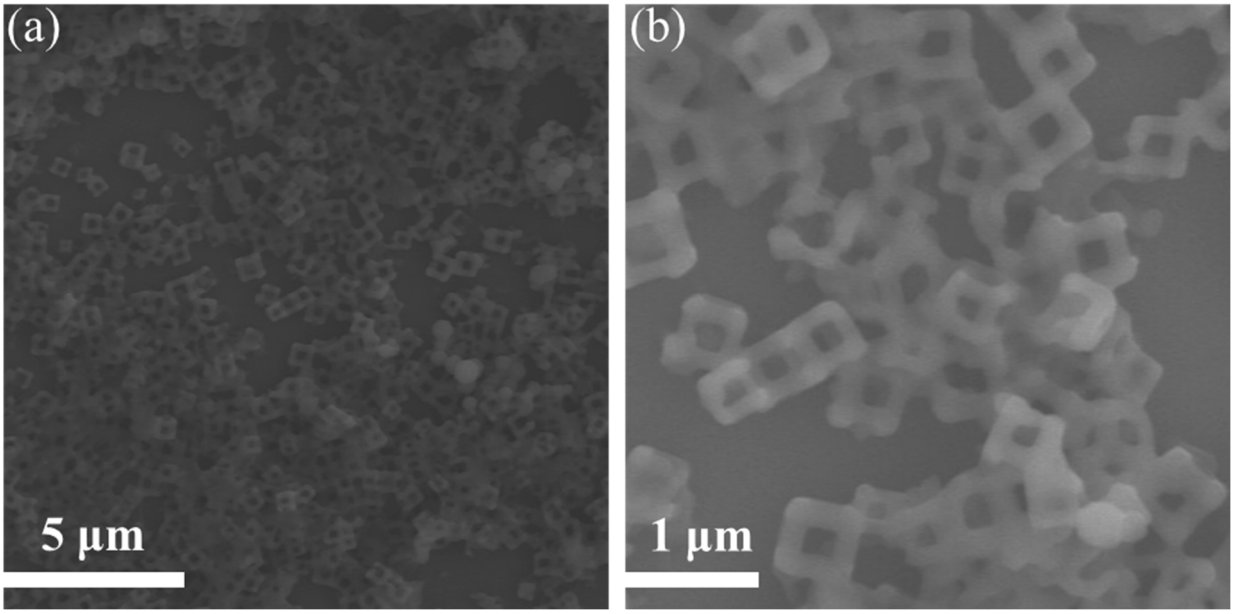

Figure S11 SEM image of ZIF-L frames.

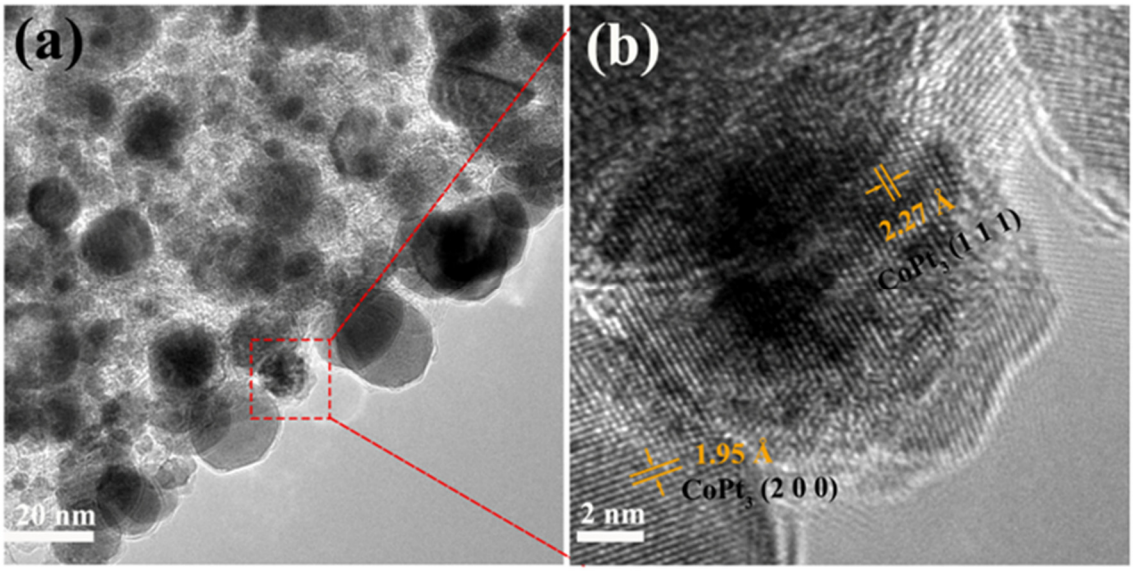

Figure S12 (a-b) HR-TEM images of $CoPt_3$@NC-NFs

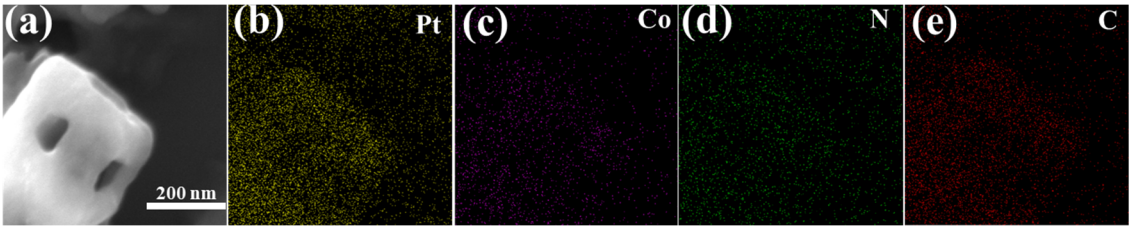

Figure S13 (a) HAADF-STEM images, and (b-e) EDS elemental mapping of $CoPt_3$@NC-NFs.

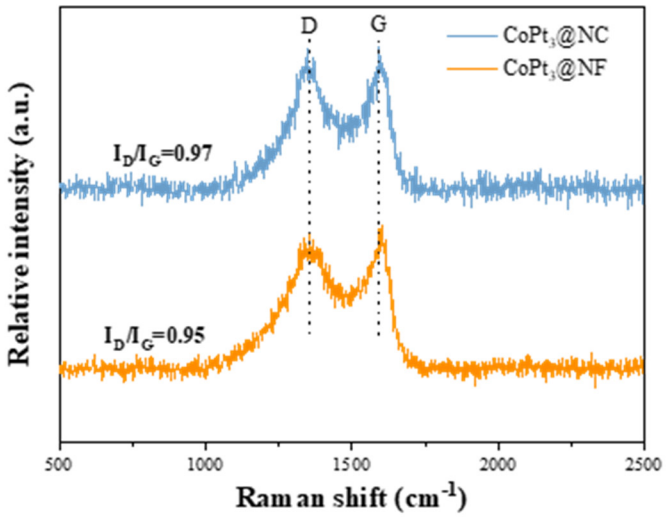

Figure S14 Raman spectra of $CoPt_3$@NC-NFs and $CoPt_3$@NC.

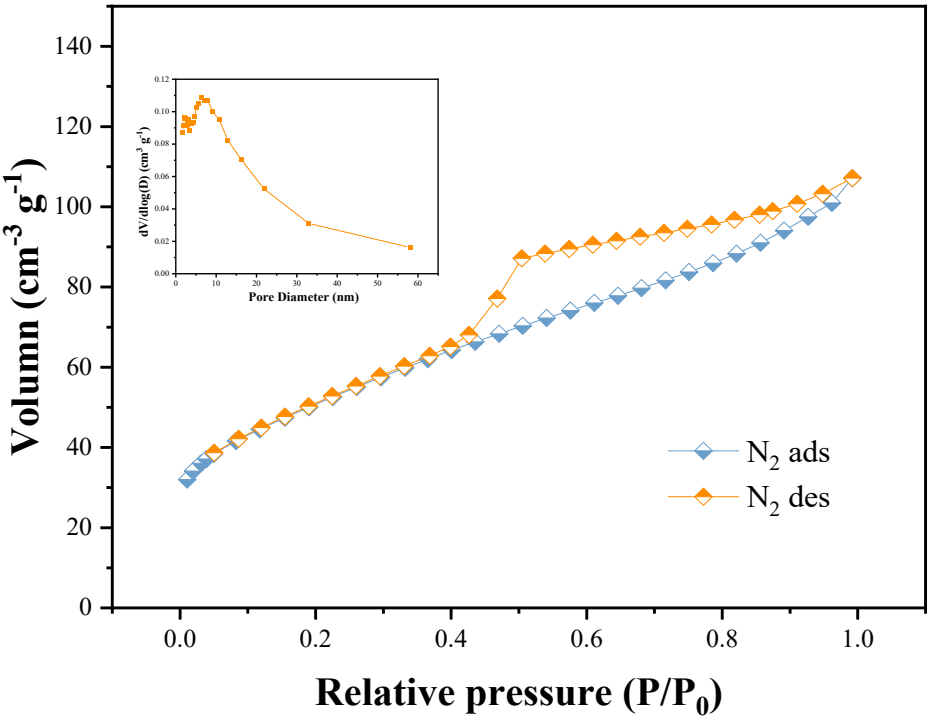

Figure S15 N_2 adsorption-desorption isotherms of $CoPt_3$@NC-NFs (inset: pore size distribution)

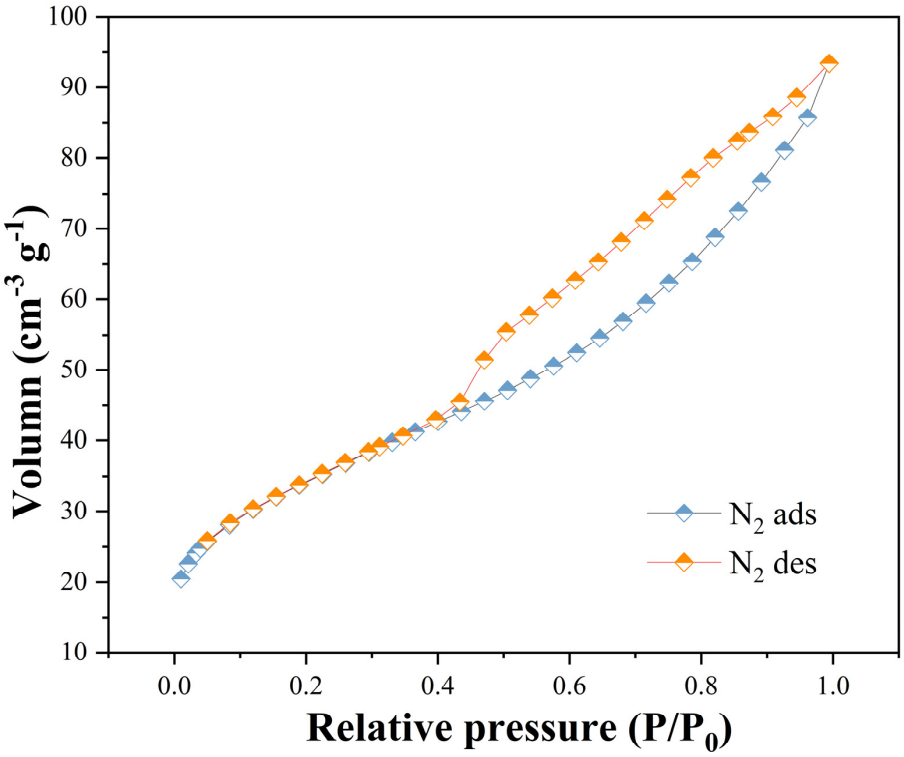

Figure S16 N_2 isothermal adsorption and desorption diagram of $CoPt_3$@NC.

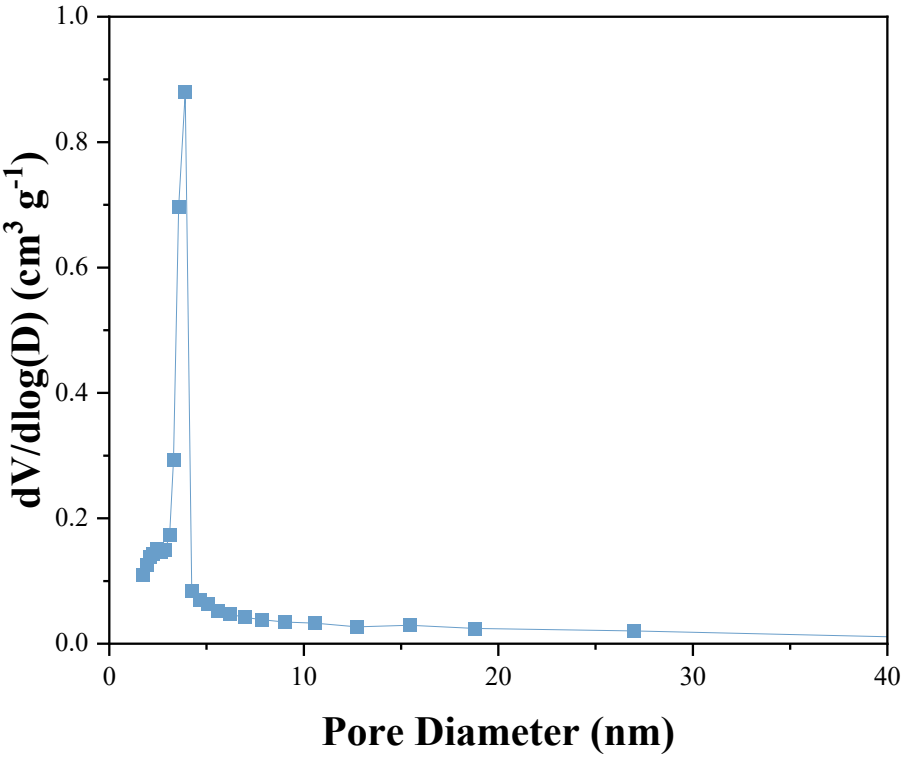

Figure S17 The pore size distribution of $CoPt_3$@NC.

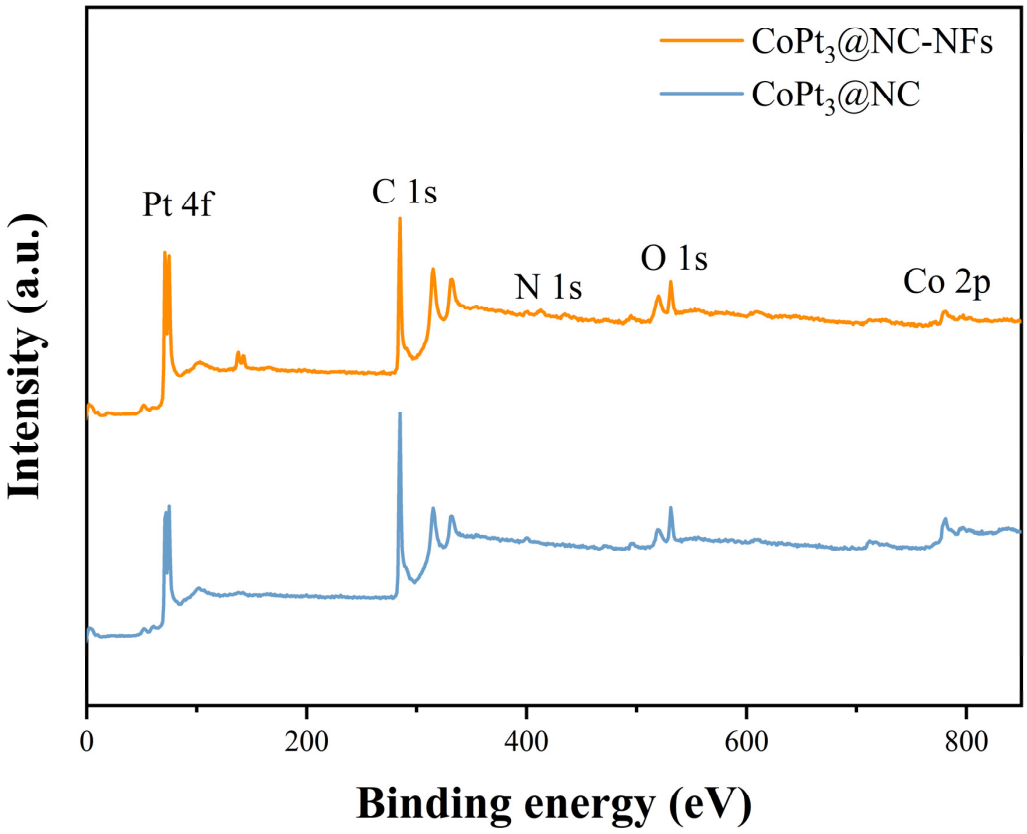

Figure S18 XPS full spectra of $CoPt_3$@NC-NFs and $CoPt_3$@NC.

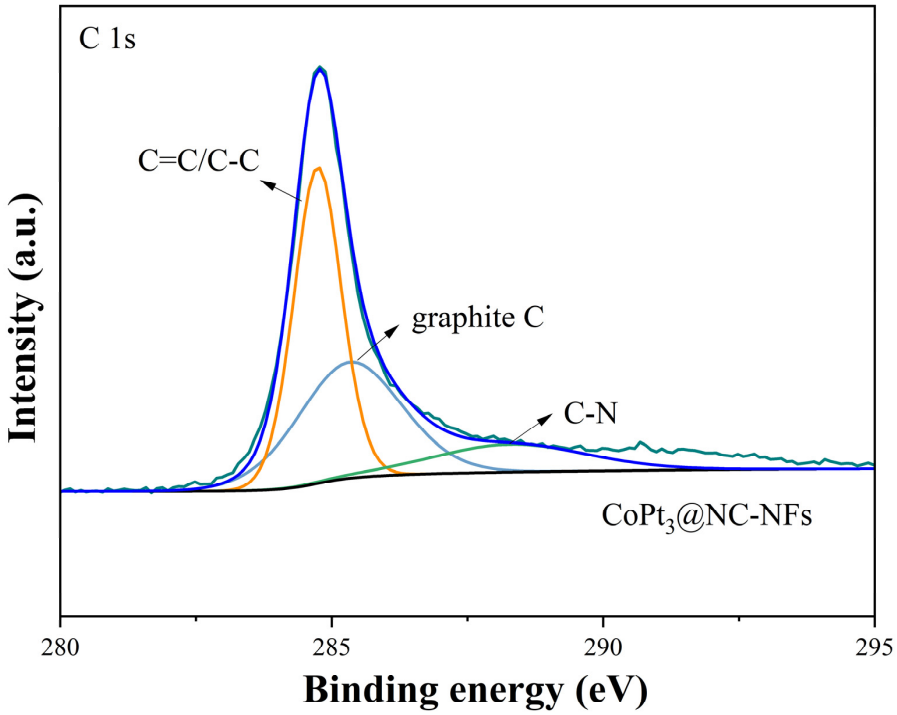

Figure S19 XPS spectrum of C 1s from $CoPt_3$@NC-NFs.

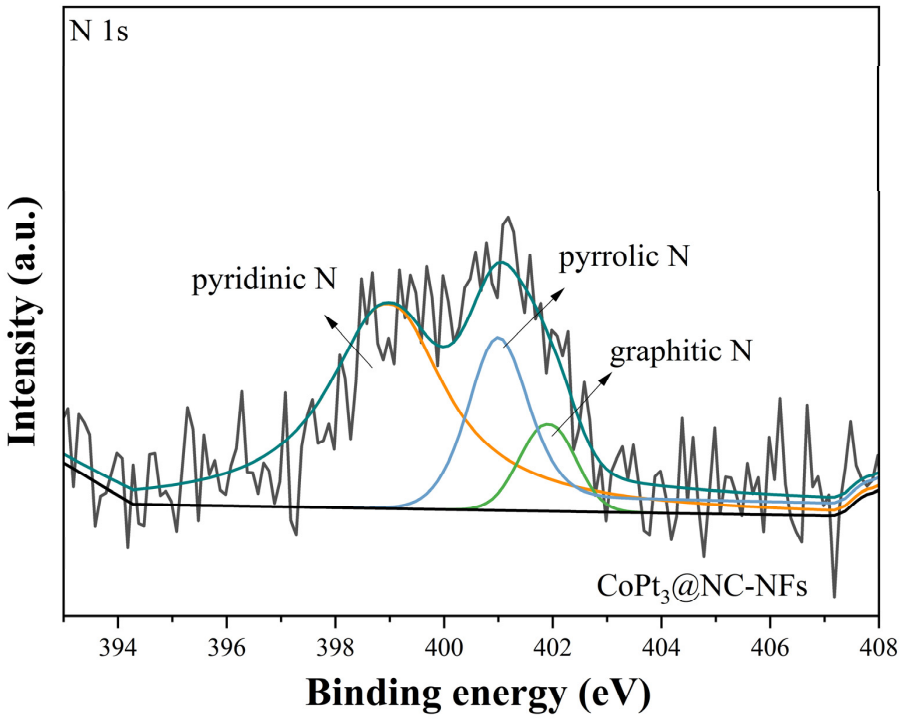

Figure S20 XPS spectrum of N 1s from $CoPt_3$@NC-NFs.

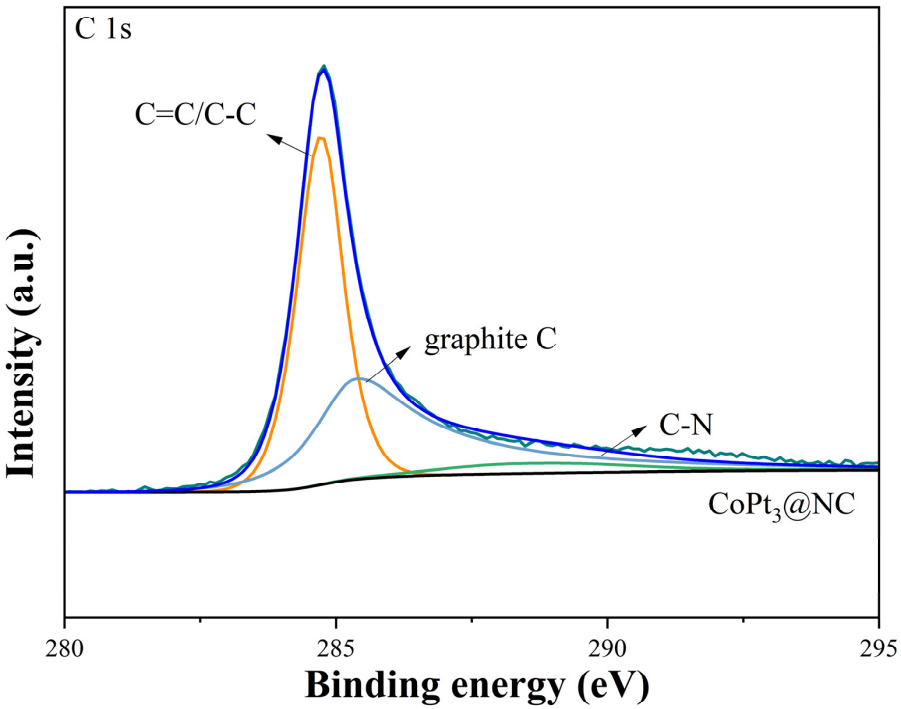

Figure S21 XPS spectrum of C 1s from $CoPt_3$@NC.

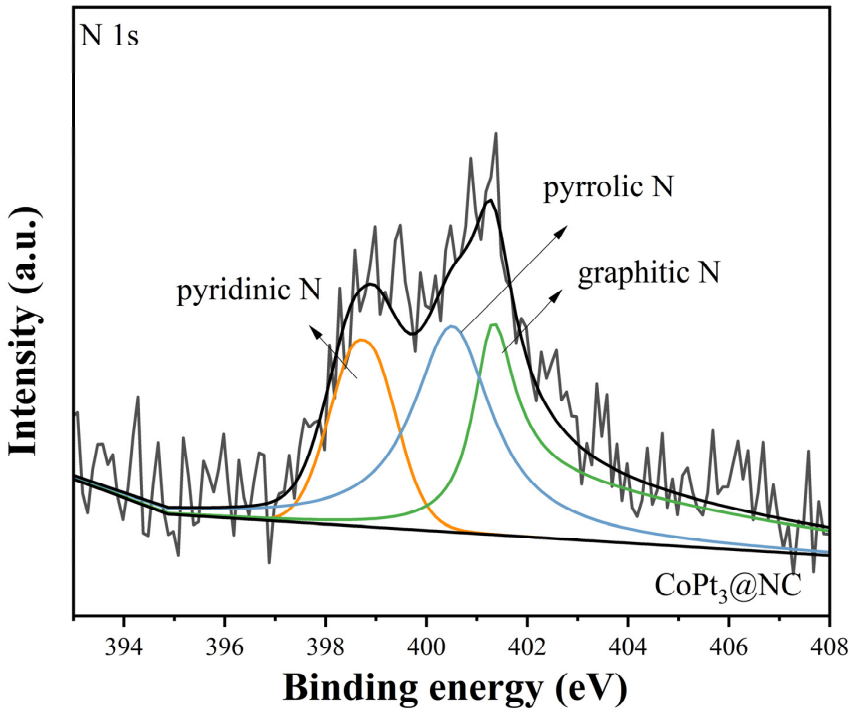

Figure S22 XPS spectrum of N 1s from $CoPt_3$@NC.

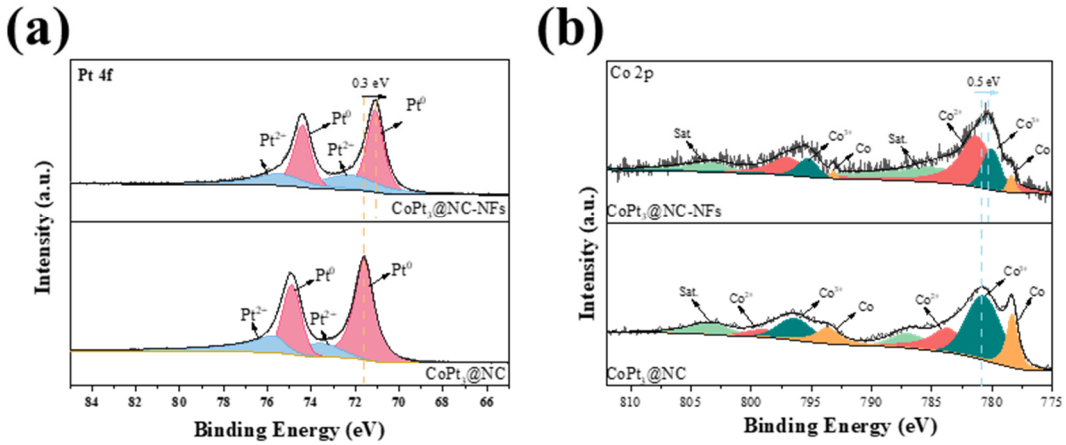

Figure S23 High-resolution XPS spectra of Pt 4f (a) and Co 2p (b) for $CoPt_3$@NC-NFs and $CoPt_3$@NC.XPS spectrum of N 1s from $CoPt_3$@NC.

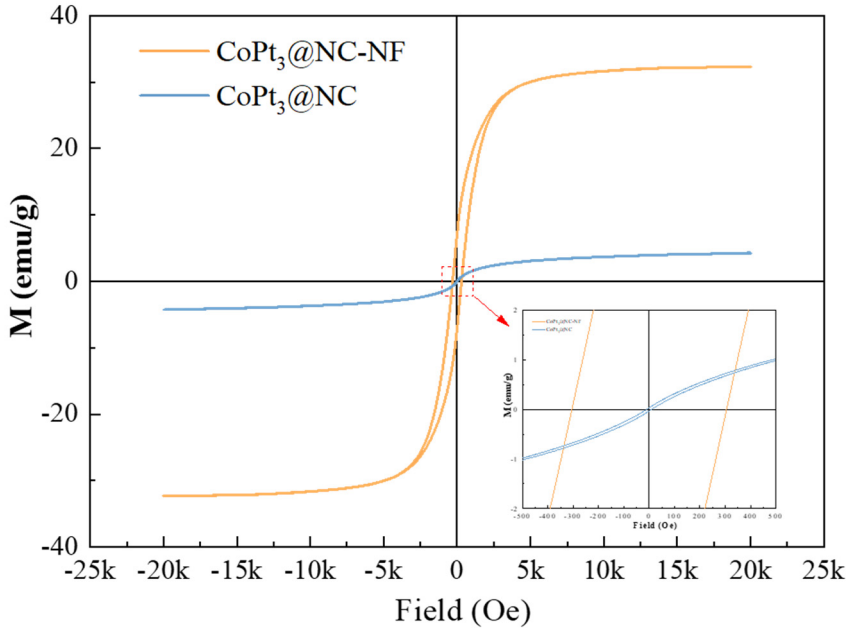

Figure S24 Hysteresis loops of $CoPt_3$@NC-NFs and $CoPt_3$@NC.

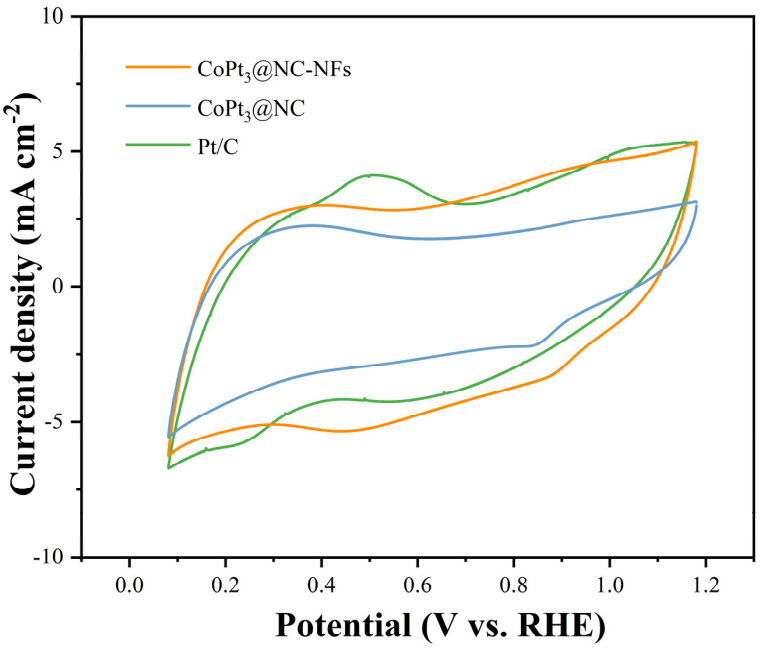

Figure S25 CV diagrams of various $CoPt_3$-based materials and Pt/C.

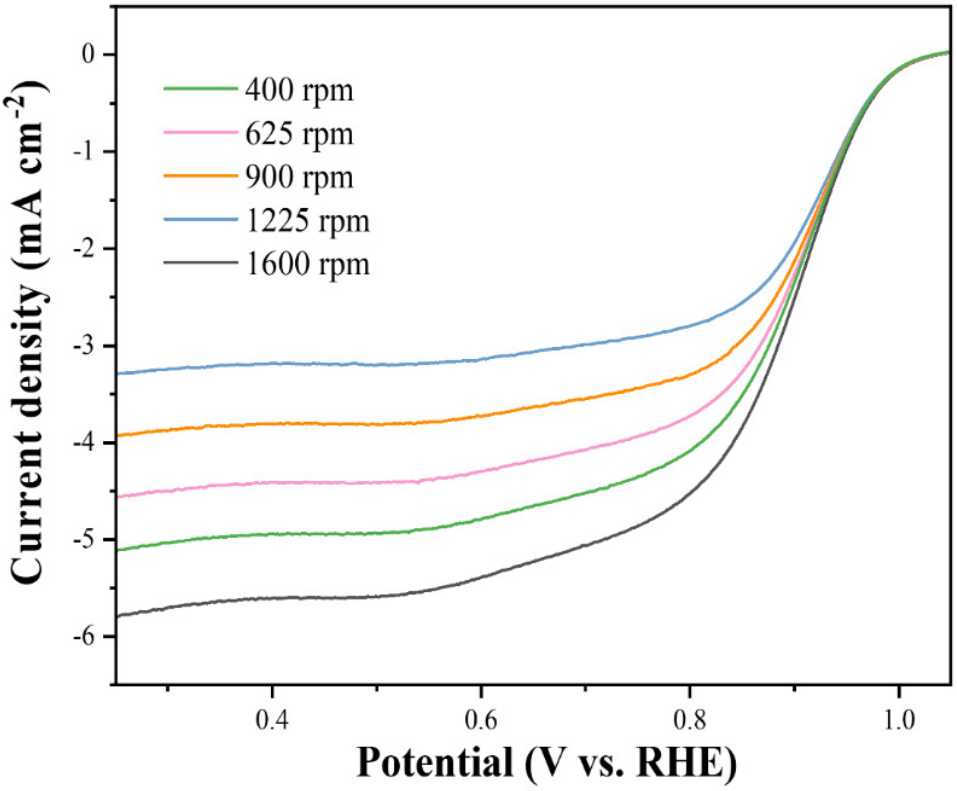

Figure S26 LSV diagram of $CoPt_3$@NC-NFs at different rotation rates

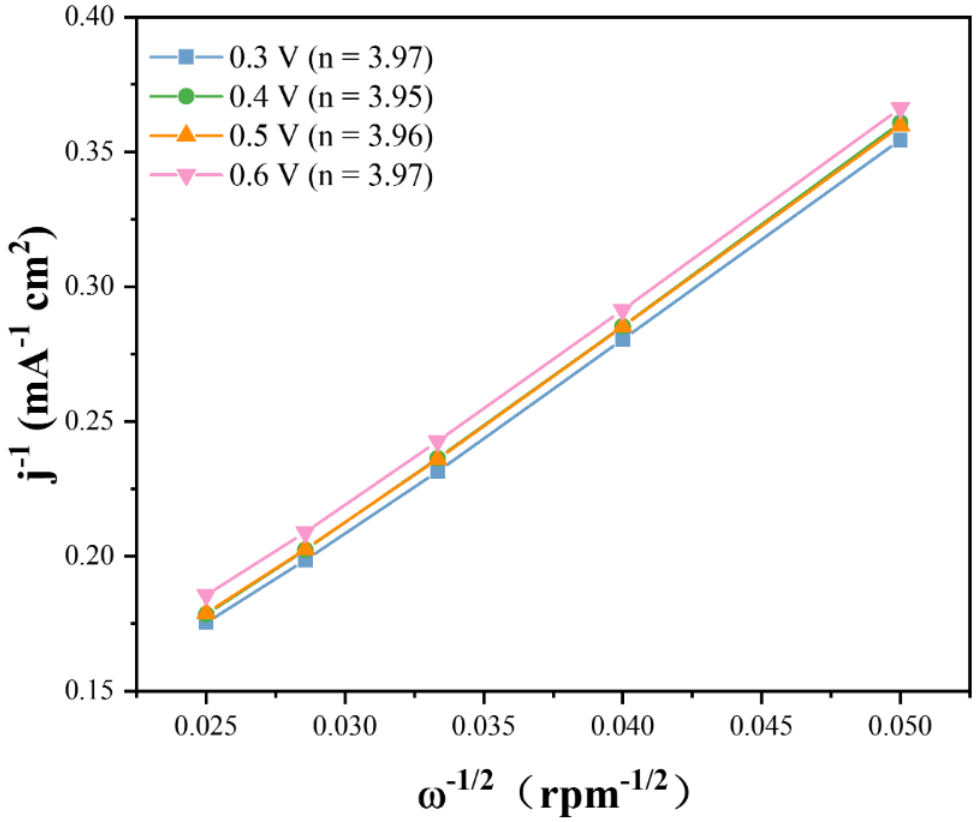

Figure S27 K-L curve under different potential of $CoPt_3$@NC-NFs.

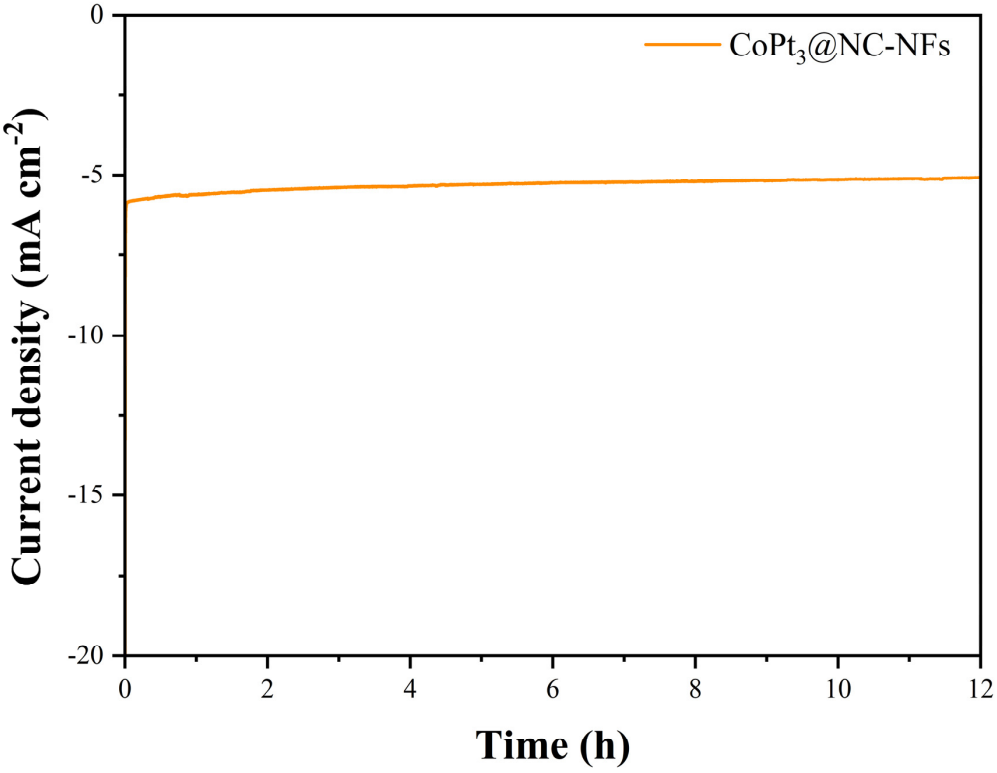

Figure S28 Current versus time (*i*–*t*) test of the $CoPt_3$@NC-NFs at 0.3 V in O_2-saturated 0.1 M KOH.

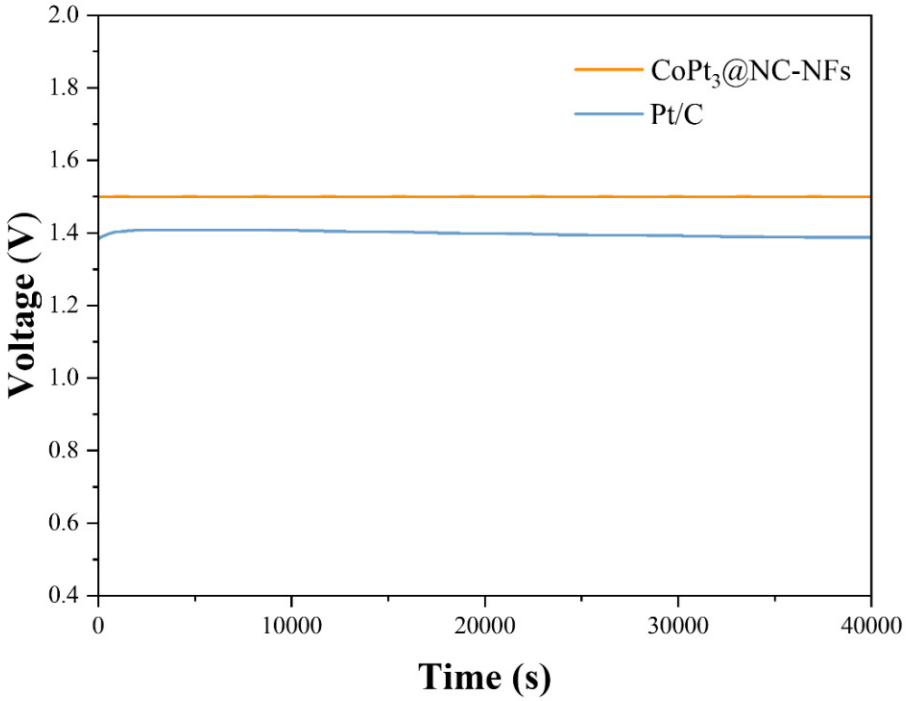

Figure S29 Open circuit voltage of NF and Pt/C-based ZABs.

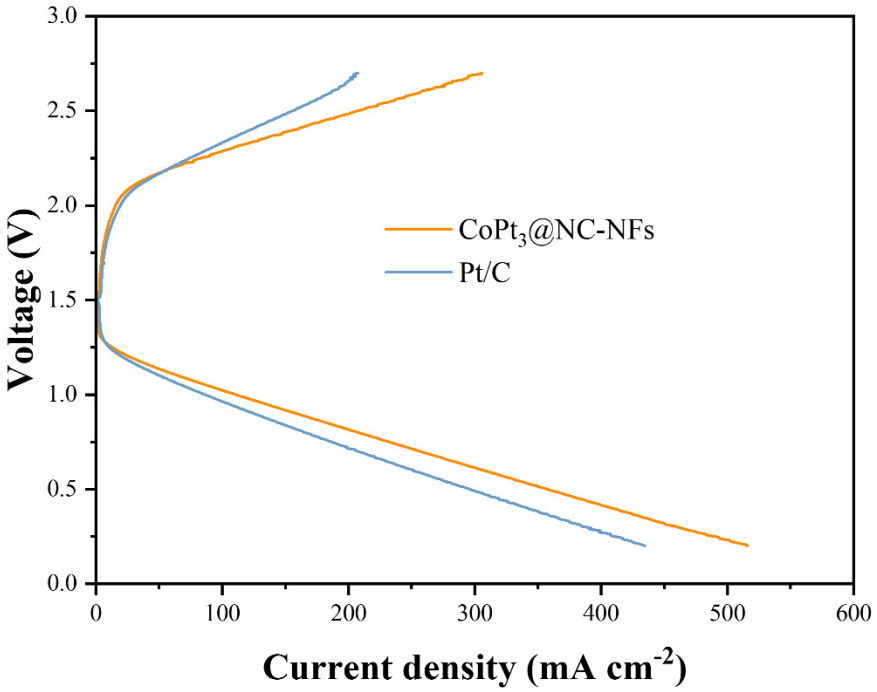

Figure S30 Charge-discharge polarization curves.

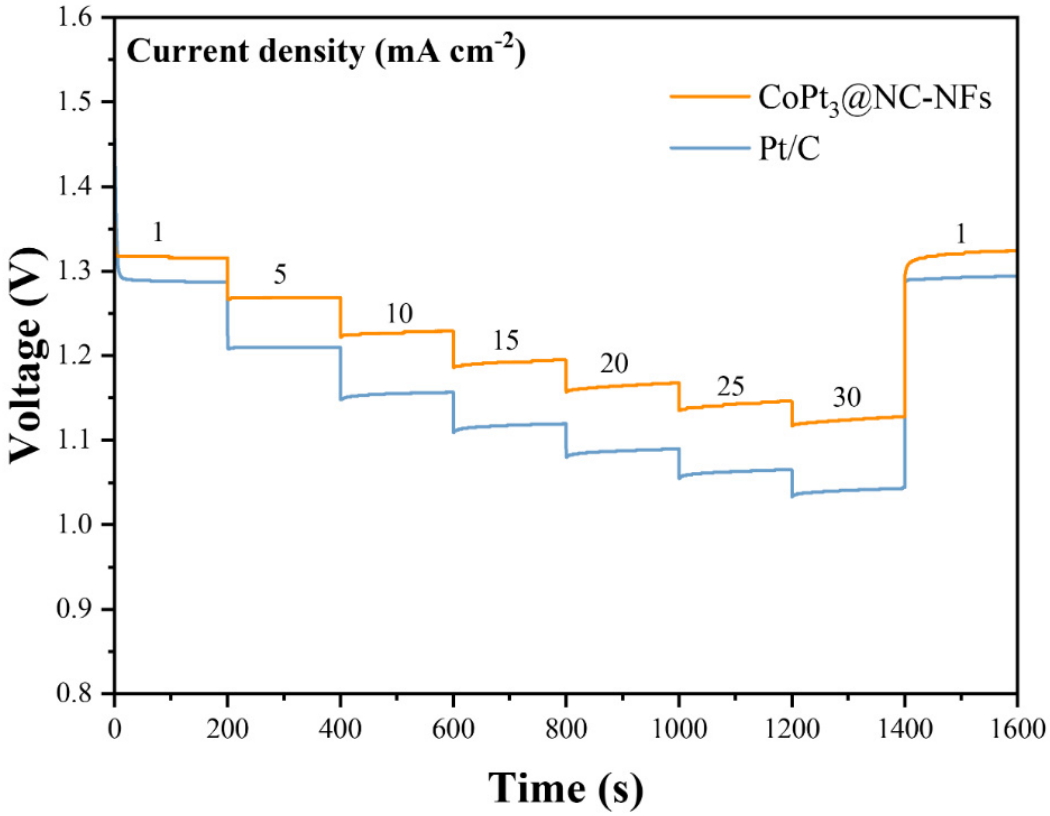

Figure S31 Discharge curves of NF and Pt/C-based ZABs at different current densities;

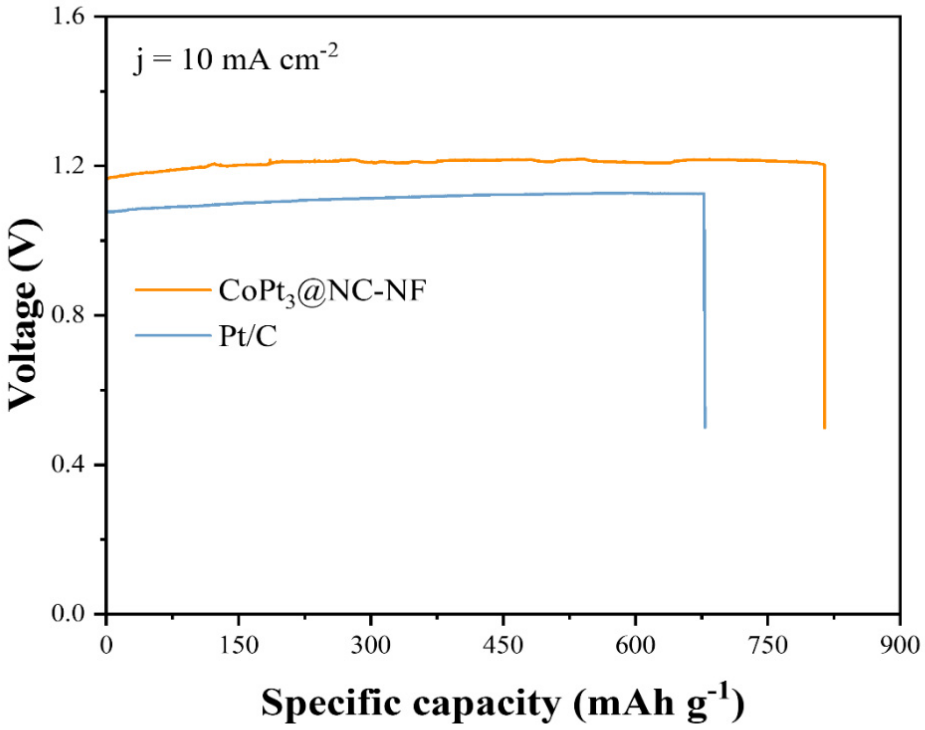

Figure S32 Specific capacities of NF and Pt/C-based ZABs;

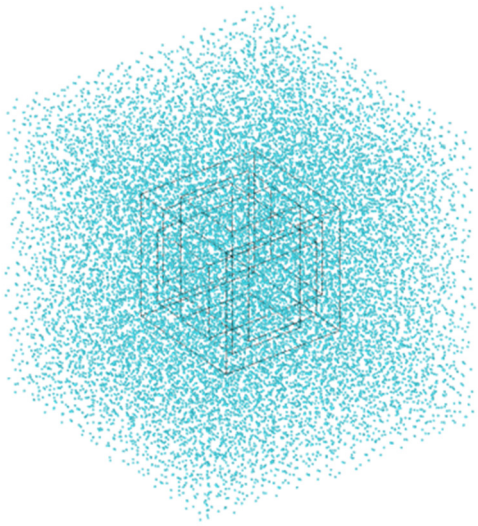

.

Figure S33 Diffusion distribution model of O_2 molecules within the framework model.

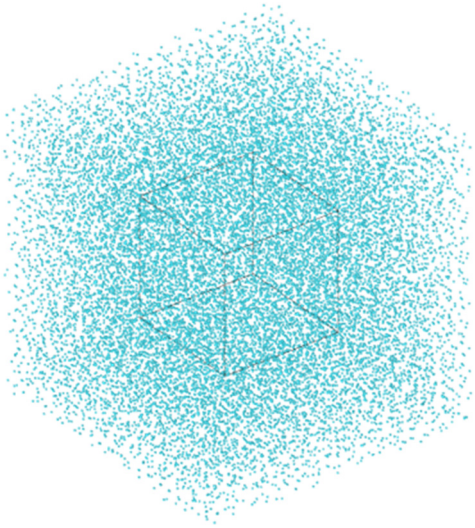

Figure S34 Diffusion distribution model of O_2 molecules within the cubic model.

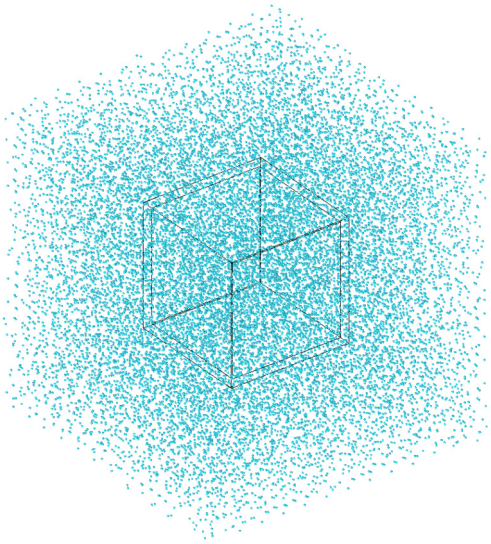

Figure S35 Diffusion distribution model of O_2 molecules within the hollow model.

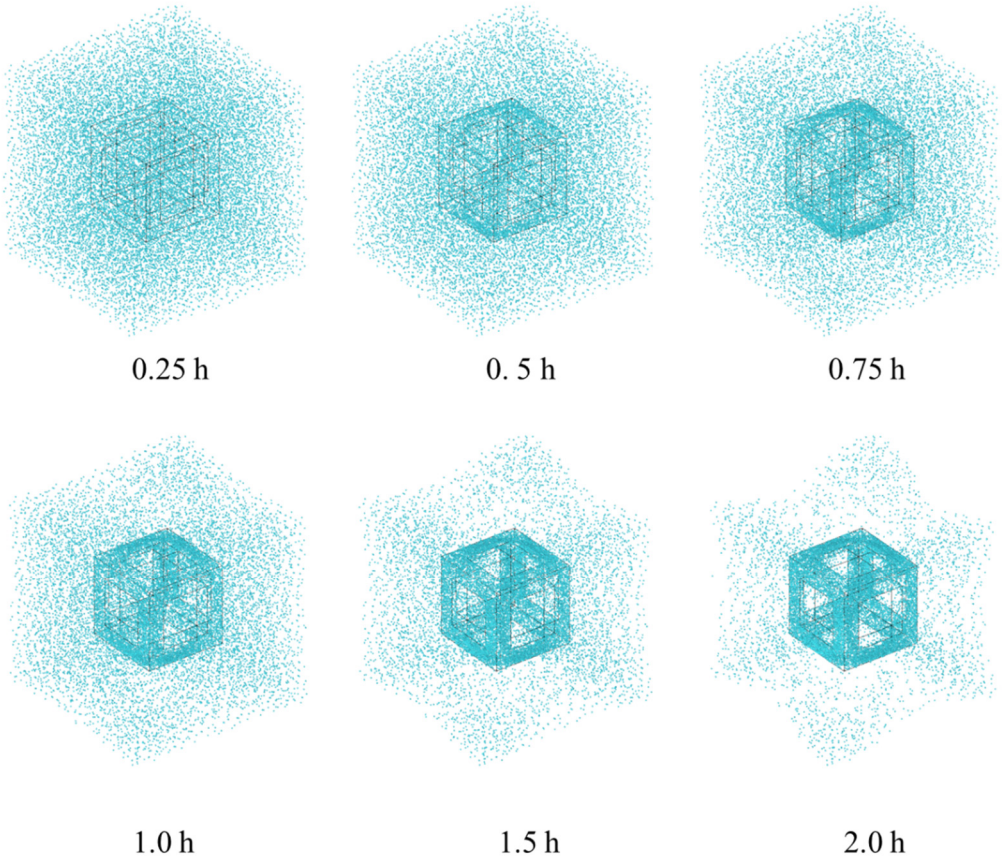

Figure S36 The distribution of O_2 molecules around frame model at different times at 7 nA.

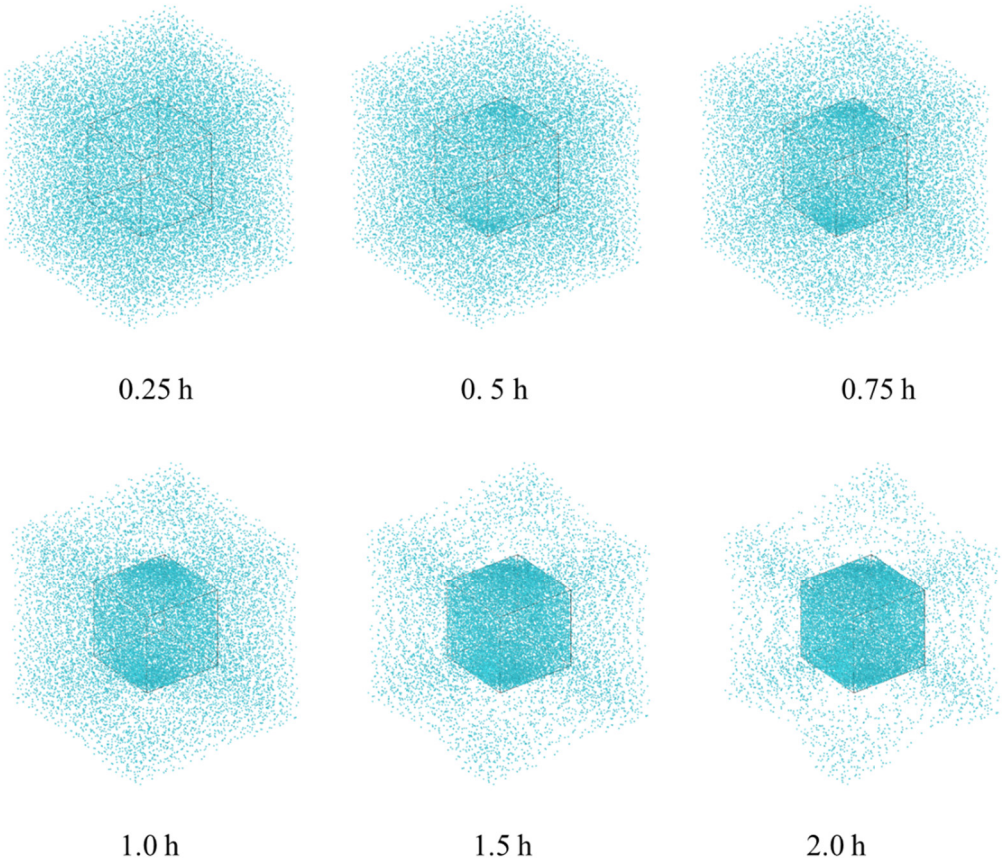

Figure S37 The distribution of O_2 molecules around cubic model at different times at 7 nA.

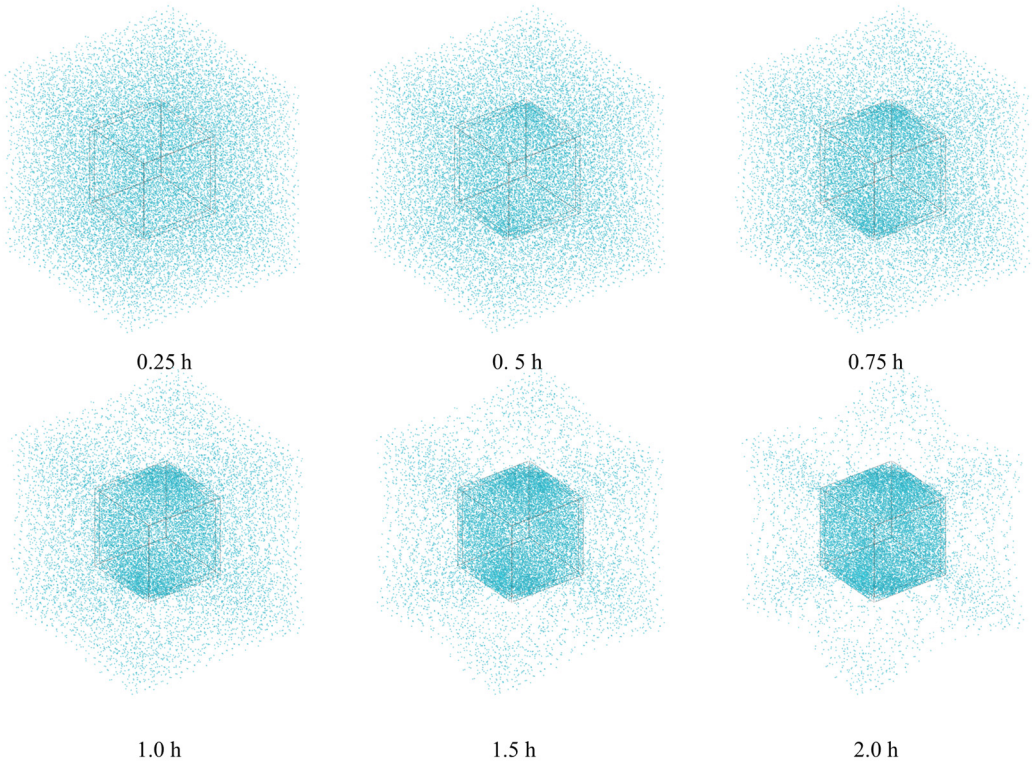

Figure S38 The distribution of O_2 molecules around hollow model at different times at 7 nA.

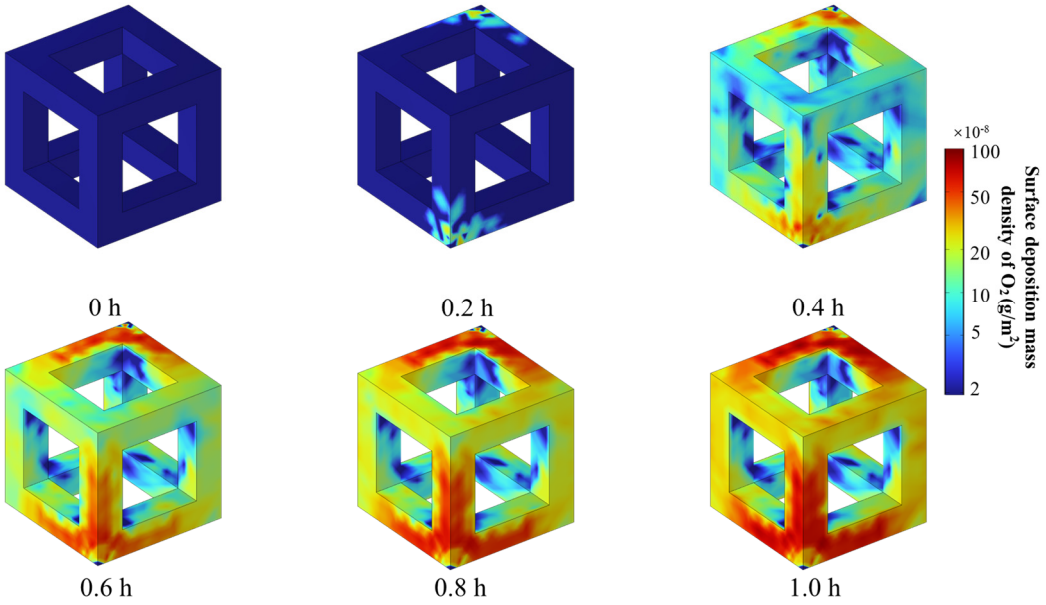

Figure S39 The deposition distribution of O_2 molecules on the surface of the frame model.

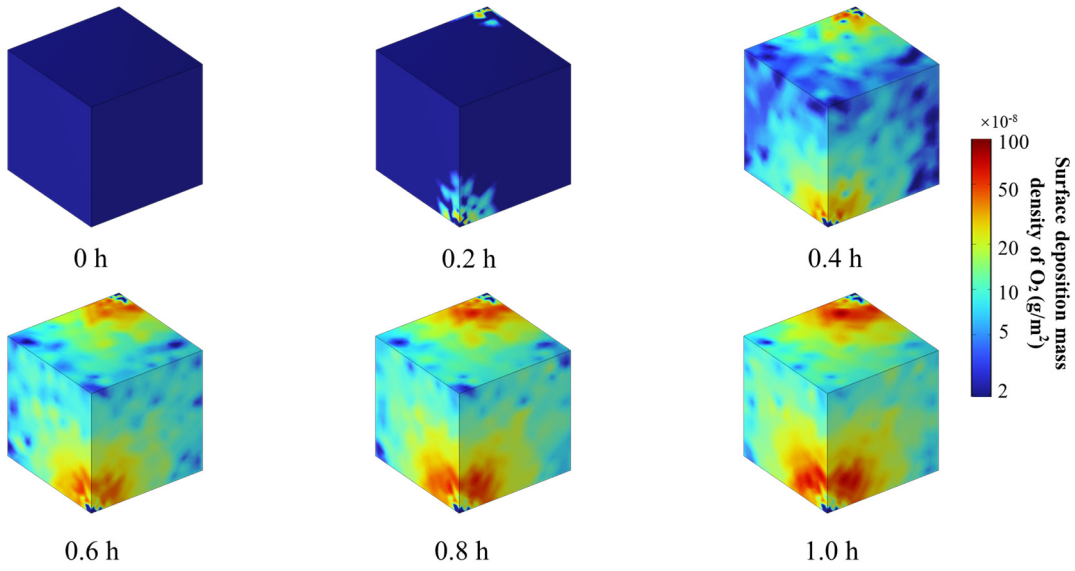

Figure S40 The deposition distribution of O_2 molecules on the surface of the cubic model.

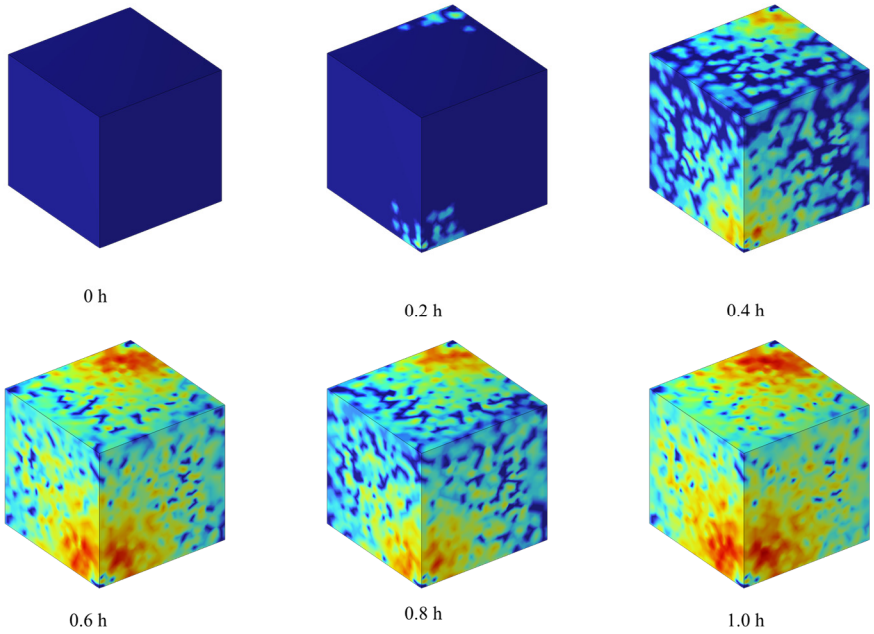

Figure S41 The deposition distribution of O_2 molecules on the surface of the hollow model.

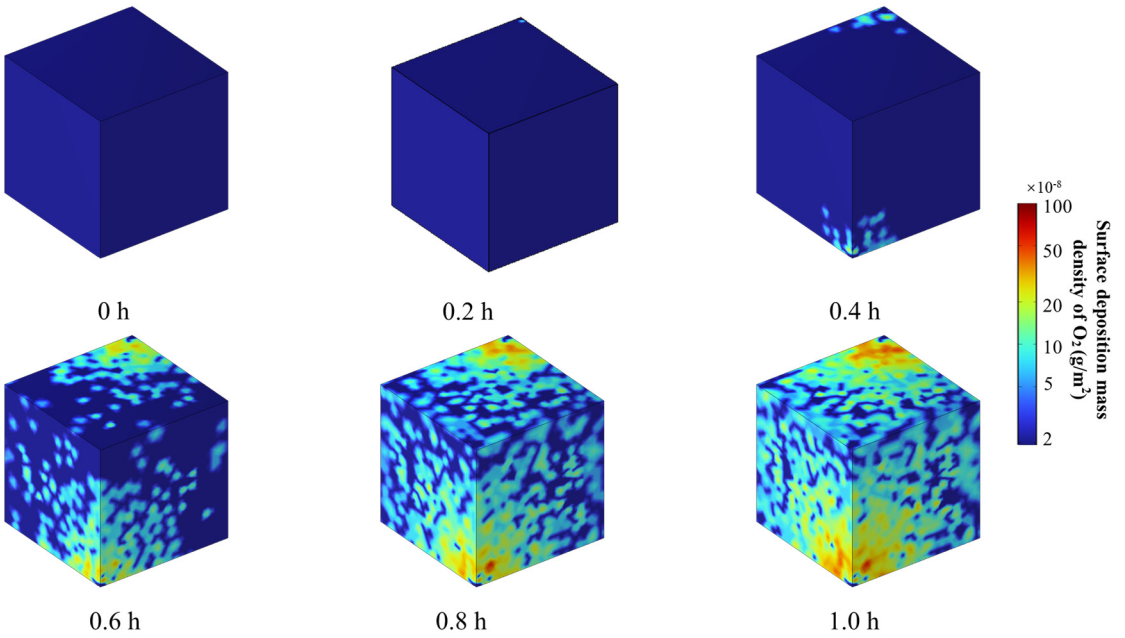

Figure S42 The deposition distribution of O_2 molecules on the surface of the hollow model

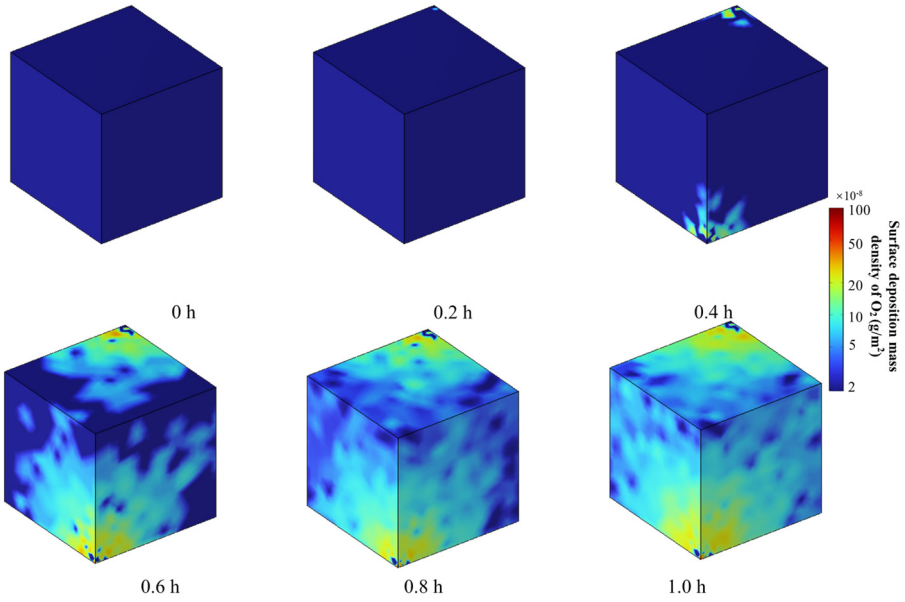

Figure S43 The deposition distribution of O_2 molecules on the surface of the cube model

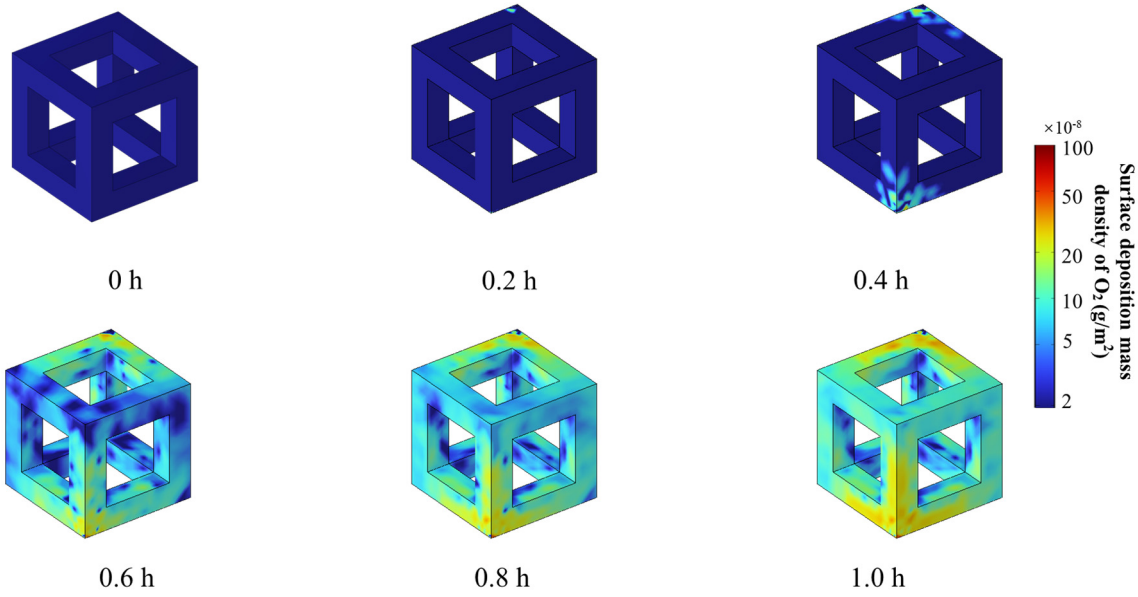

Figure S44 The deposition distribution of O_2 molecules on the surface of the frame model

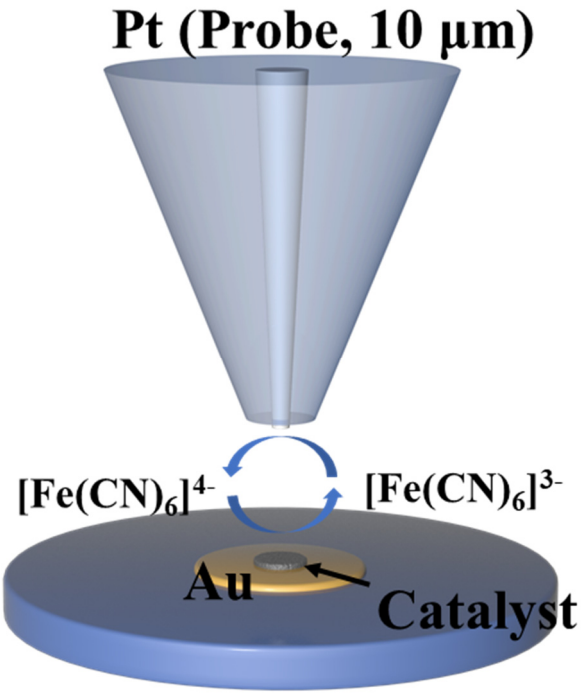

Figure S45 The charge transfer process at the interface of tip and substrate electrode surface.

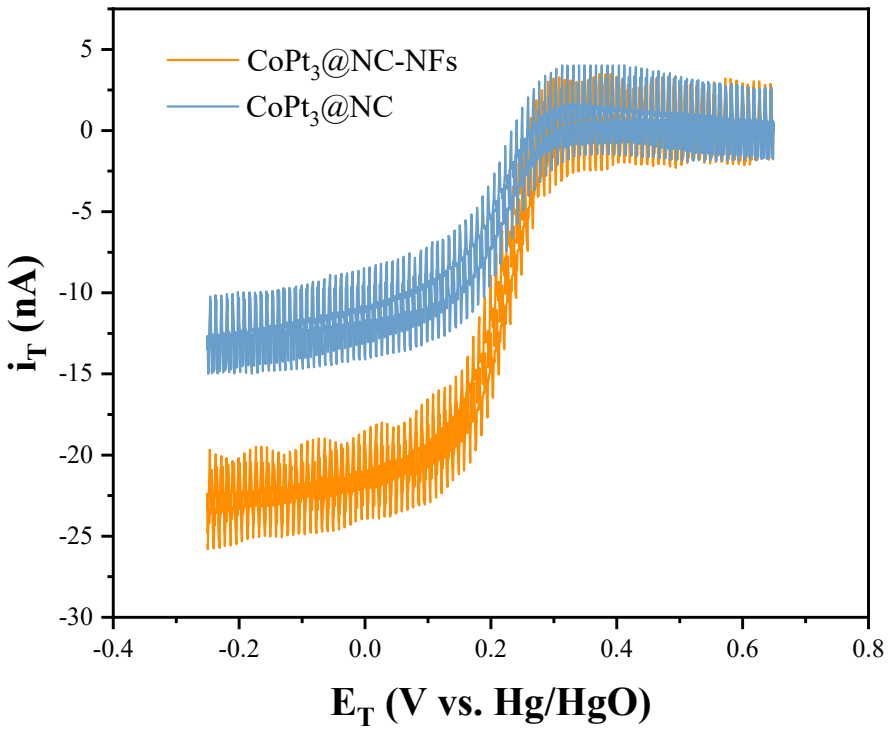

Figure S46 CVs recorded at the SECM tip over both the $CoPt_3$@NC-NFs and $CoPt_3$@NC in 0.01 M $K_3[Fe(CN)_6]$ and 0.1 M KCl mixed electrolyte at the scan rate of 50 mV s^{-1}.

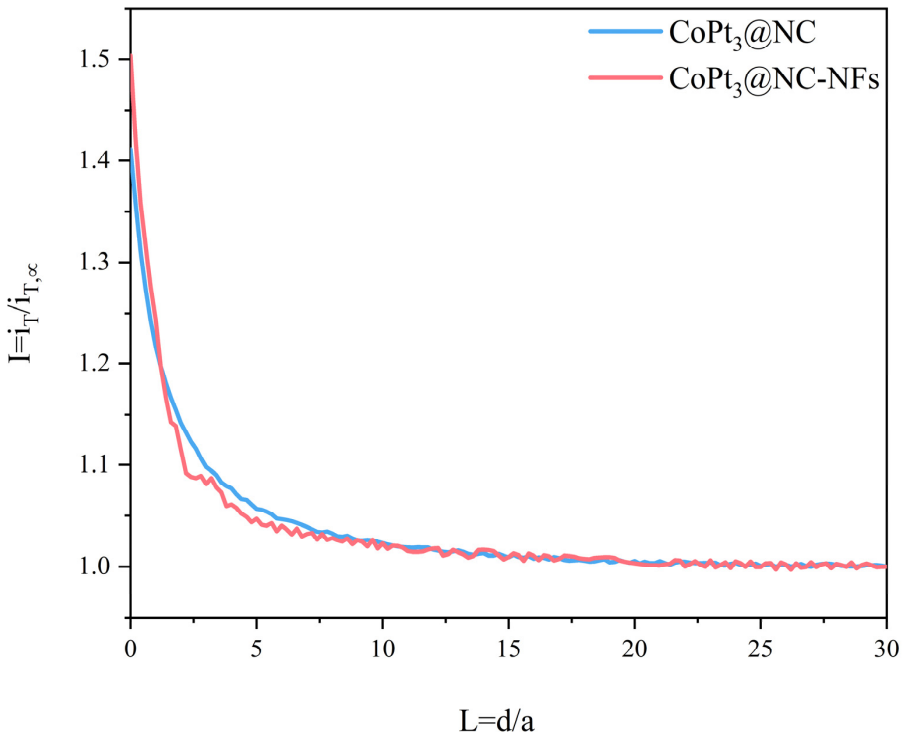

Figure 47 SECM tip approach curves (PACs) of $CoPt_3$@NC and $CoPt_3$@NC-NFs [E_T= −0.3 V, E_S (OCV)].

Table S1 Element concentrations in different samples determined by XPS analysis

	Pt (at %)	Co (at %)	C (at %)	O (at %)	N (at %)
$CoPt_3$@NC-NFs	7.84	2.62	80.28	7.42	1.84
$CoPt_3$@NC	5.5	1.93	82.75	7.17	2.23

References

1. Kresse G, Furthmüller J. Efficient iterative schemes for ab initio total-energy calculations using a plane-wave basis set. *Physical Review B* 1996, **54**(16)**:** 11169-11186.
2. Blöchl PE. Projector augmented-wave method. *Physical Review B* 1994, **50**(24)**:** 17953-17979.
3. Perdew JP, Burke K, Ernzerhof M. Generalized Gradient Approximation Made Simple. *Phys Rev Lett* 1996, **77**(18)**:** 3865-3868.
4. Kresse G, Furthmüller J. Efficiency of ab-initio total energy calculations for metals and semiconductors using a plane-wave basis set. *Computational Materials Science* 1996, **6**(1)**:** 15-50.